One-dimensional model and solutions for creeping gas flows in the approximation of uniform pressure

A. Vedernikov[1,*] and D. Balapanov[1,2,†]
[1]*Microgravity Research Center, Université Libre de Bruxelles, 1050 Brussels, Belgium*
[2]*Institute of Mechanics, Ufa Branch of RAS, 450054 Ufa, Russia*
(Received 25 March 2016; published 29 November 2016)

A model, along with analytical and numerical solutions, is presented to describe a wide variety of one-dimensional slow flows of compressible heat-conductive fluids. The model is based on the approximation of uniform pressure valid for the flows, in which the sound propagation time is much shorter than the duration of any meaningful density variation in the system. The energy balance is described by the heat equation that is solved independently. This approach enables the explicit solution for the fluid velocity to be obtained. Interfacial and volumetric heat and mass sources as well as boundary motion are considered as possible sources of density variation in the fluid. A set of particular tasks is analyzed for different motion sources in planar, axial, and central symmetries in the quasistationary limit of heat conduction (i.e., for large Fourier number). The analytical solutions are in excellent agreement with corresponding numerical solutions of the whole system of the Navier-Stokes equations. This work deals with the ideal gas. The approach is also valid for other equations of state.

DOI: 10.1103/PhysRevE.94.053121

I. INTRODUCTION

Compressible fluid dynamics is most often associated with high-velocity gas motion. However, the compressibility may be a key factor in a wide class of arbitrarily slow flows, when the essential part of the flow occurs in a small enough domain, in which the pressure equalization time is much shorter than the characteristic time of the density variation. Then, the pressure may be treated as uniform over the whole task region, while the other thermodynamic parameters vary (homobaric approximation). Gas motion around or inside a slowly expanding bubble or around a droplet with surface temperature variation and/or interfacial mass exchange are the illustrative snapshots from the class of such tasks.

In many circumstances, the creeping gas flows have high symmetry, so that at least locally the flow may be considered as unidirectional. Symmetry of the flow and uniformity of the pressure facilitate finding analytical solutions for the gas velocity profiles, which is the goal of the paper.

A. Precedent theoretical studies

Surprisingly, only a few analytical studies of the velocity fields in the homobaric approximation have been conducted. The pioneering theoretical work was done by Lord Rayleigh [1], who took into consideration the influence of gas density variation on heat transfer in a gas. He found an analytical solution describing one-dimensional heat transfer in a spherical layer of air in the absence of mass forces. The solution was obtained from a linearized energy equation under the assumption of uniform pressure. The equation of state was taken to be linear instead of using the ideal gas equation, and the solution was obtained only for the temperature profile, assuming that gas displacement does not influence the heat propagation. This simple model served as a starting point in the investigation of thermoacoustic phenomena.

In Ref. [2], Lord Rayleigh's solution was improved by adding the integral mass conservation equation to find the pressure as a function of time. It was noted that the homobaric approximation excludes acoustic waves from the solution. The numerical solution of the updated model substantially deviated from the numerical solution of the conservation equation system with nonuniform pressure and an advective term in the energy equation. In Ref. [3], the above mentioned discrepancy is attributed to an inaccurate computational scheme.

Using boundary layer analysis and time-scale decomposition, the authors of Refs. [3,4] studied the subsidence to thermal equilibrium of a confined ideal gas at slow and rapid boundary heating. An analytical solution was obtained in the form of a power series with the Mach number being a small parameter. Their works laid a sound foundation for thermoacoustic wave investigation at a relatively fine time scale.

In Refs. [5–7], only the first-order Mach number components were retained in the momentum and energy equations, establishing the basis of the homobaric approximation. The approach appeared to be quite productive in the general analysis of homobaric flows and enabled the development of considerably simplified numerical schemes.

The effect of gas density variation on one-dimensional heat transfer was analyzed in detail in Refs. [8–10], where moving and permeable boundaries were also considered. It was shown that the velocity may be excluded from the full system of equations by formal mathematical transformations [6,9]. Nevertheless, most of their solutions were obtained numerically, focused on the influence of advection on heat propagation. Dimensionless criteria for the validity of the heat conduction equation in compressible flows were developed in Ref. [10] and are applied and discussed in Sec. II A of this article. The smallness of the kinetic energy as compared to the variation of the total energy was proposed as an alternative criterion in justifying the use of homobaric approximation. It was pointed out that in view of the thermal phenomena description, the homobaric approximation plays an intermediate role between

*avederni@ulb.ac.be
†dbalapan@ulb.ac.be

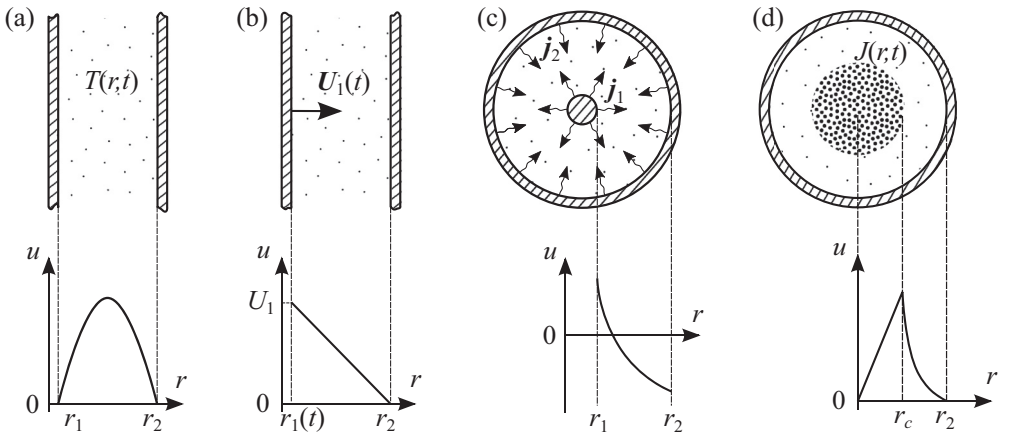

FIG. 1. Gas flow sources in different geometries and typical flow velocity profiles: (a) a cavity with temperature variation on the walls; (b) moving boundary; (c) gas inflow and outflow on the boundaries; and (d) distributed mass source of heat and/or mass.

the thermodynamics and the full theory of heat transfer in gases. The equation system was generalized for chemically reacting gas mixtures in Refs. [6,7,11].

Analytical solutions for the velocity field are in great need because solving the full system of conservation equations for the compressible media at low Mach number by existing numerical methods requires enormous computing resources. In this paper, we further simplify the above referenced works by excluding the advection term from the energy equation. This allowed us to obtain the analytical solution for the gas velocity.

B. Examples of high-symmetry gas creep flows

Before proceeding to the formulation of the model and analysis of the solutions, we present typical examples of pertinent flows to give a better view of the diversity of tasks and possible application of the results. First, we illustrate the variety of the gas motion sources and geometries, assuming that the influence of the mass forces is negligible.

Among the most frequent realizations is the time-dependent temperature profile $T(r,t)$ in the region limited by two boundaries, as shown in Fig. 1(a). The nonstationary, nonuniform temperature modifies the gas density field, leading to gas displacement with a typical velocity profile as presented below on the same figure. The animation in the Supplemental Material [12] presents an example flow in a planar gap induced by variation of the temperature of one of the planes. This thermally driven motion is well manifested in microgravity conditions, in absence of natural convection, which prevails at normal gravity.

One or both boundaries may move, as shown in Fig. 1(b). Gas flow through one or both boundaries is another source of the gas motion, as illustrated in Fig. 1(c) in the axially symmetric case, top view. Particularly, it happens between permeable tubes or for the phase transition on the boundaries.

Finally, the source that modifies the gas density may be distributed in the volume. A cloud of microscopic particles floating in a spherical cavity illustrates such systems, as shown in Fig. 1(d). In the latter case, the gas motion starts when the cloud is subjected, for example, to the external illumination that heats the particles and consequently modifies the temperature profile in the gas. The particles also may be a source of gas mass variation due to phase transition, chemical reaction, etc.

1. *Fuel tanks of space vehicles*

The reduced-gravity environment requires consideration of the nongravity sources of fluid motion [13]. The first quantitative analysis having practical interest and experimental verification was said to have been done during the Apollo space program [2,14,15], targeting transient processes in a cryogenic propellant tank or the sizing of supercritical storage systems. In these tasks, gas motion resulted from the variation of gas density because of varying boundary temperature. The main interest in these and later papers was related to the extreme cases of thermally driven pressure variation generating thermoacoustic waves or the "piston effect" in fluids near the critical point [16,17]. However, the study in this paper is limited to the uniform pressure condition.

2. *Measurement of aerosol particle transport properties*

In the area of aerosol sciences and dust cloud mechanics, measurement of particle transport properties is of basic importance, as they define the forces in the equation of particle motion. The particle velocities ideally should be measured in the reference frame of gas, while in reality the measurements are done in the fixed laboratory reference frame. In all such experiments, the gas creep is inevitable, and the velocity field should be well defined. The capacitor-type geometry of the cell, as in Fig. 1(a), is used in many microgravity experiments on thermophoresis [18–26] and diffusiophoresis [25], where the top and bottom plates were at different temperatures or provided the diffusive matter flux from one plate to the other. Investigation of negative thermophoresis was performed in the axisymmetric geometry in Refs. [27,28]. Transition from normal gravity to microgravity in the drop tower flight led to small but not negligible temperature variation in the cell and thus that of the gas density field. In the latter experiments, for example, the velocity accuracy should be on the order of 1 μm/s so that even the slightest gas motion should be considered.

3. Moving boundaries and boundary mass sources

Piston displacement, as shown in Fig. 1(b), is a typical presentation of one-dimensional gas flow, assuming that the piston moves slowly enough and lateral boundaries are sufficiently far. In applications, this task may be complicated by the presence of a temperature profile varying in time and eventual volumetric and/or boundary gas sources.

A bubble or a droplet with a varying diameter and, eventually, with varying temperature, and evaporation or condensation on the boundary and in the gas, represents a centrosymmetric analog of the previous example. Burning droplets have been a subject of many microgravity experiments [29] related to the gas motion in the external region with respect to the boundary. An example of the internal task is illustrated by the experiments on measurement of evaporation and condensation coefficients in the spherical chamber of fixed diameter, with the source of the investigated substance deposited on the internal chamber surface [30].

Homobaric approximation is valid for the description of acoustic cavitation and sonoluminescence of bubbles [31,32]. For example, a water vapor bubble of diameter $d = 10^{-4}$ m, oscillating in a sound field with frequency $f = 10^5$ Hz, at room temperature, has the reference time $\tau_f = 10^{-5}$ s. Reference sound propagation time in the bubble interior is $\tau_c = d/c \approx 10^{-7}$ s, which is much less than τ_f.

Permeable walls facilitate creating one-dimensional creep flows. It may be the internal region of a hollow porous sphere or, as illustrated in Fig. 1(c), a space between two plates or the inner part of a tube. The flow characteristics outside may be arbitrary, if they do not violate the symmetry limitation in the internal region.

4. Distributed sources

Such systems are quite common: in atmospheric aerosols, the microscopic droplets surround relatively big rain drops; burning droplets stay in the cloud of particles of burning products, also participating in mass and heat transfer. A number of microgravity experiments have been devoted to the investigation of dust clouds simulating protoplanetary matter formation [33] and to the investigation of complex plasma [34,35]. Typically, the micron-sized particles form a centimeter-sized cloud, filling only the central part of a chamber, schematically presented in Fig. 1(d). In photophoretic experiments, the intensive infrared light illuminates the cloud. Upon introducing the illumination, particles heat the gas, leading to its expansion in the central part. Periodic temperature variation in the thermophoretic trap [36,37] results in a similar type of alternative cloud contraction-expansion motion. Silica particles, most often used in such experiments, are hygroscopic and may contain an important quantity of absorbed water, which should be in equilibrium with the vapor in the gas. Heating the gas or illuminating the particles, one can shift the equilibrium, which leads to additional absorption or desorption and thus to the gas flow.

C. Goals and short description

Examples presented in the current section illustrate one-dimensional homobaric flows of heat-conductive gas at low Mach number. The variety of such systems is characterized by the flow symmetry type (flat, axial, or spherical); quasistationary or essentially nonstationary heat propagation; type of the gas motion sources; and particular time dependencies.

The one dimensionality of the gas flow is the distinctive peculiarity of these tasks, making the momentum equation trivial. It suffices to apply the equation of state and of the mass conservation law. We propose a consistent approach to solving such tasks, and present analytical solutions and typical flow patterns.

In Sec. II, we formulate the problem, present a model, and provide a general solution of one-dimensional gas creeping flow in the approximation of uniform pressure. The general solution is presented in different forms, which later simplifies obtaining particular analytical solutions or getting solutions in the cases when not all the limitations are valid. We introduce approximations in the description of the thermal field that considerably simplify the analytics.

A set of particular exact and approximate solutions is obtained in Sec. III for a variety of gas motion sources in a closed domain: time-dependent thermal boundary conditions, moving boundaries, interfacial, and distributed matter sources. In most cases, the solutions are obtained in planar, axisymmetric, and centrosymmetric geometries. The solutions of Sec. III are obtained for quasistationary heat propagation (i.e., for large Fourier numbers $\mathrm{Fo} \gg 1$), leaving the tasks of small and intermediate Fourier numbers for subsequent publication. The discussion and conclusions are provided in the final two sections.

The material in this paper is presented in a detailed manner to facilitate practical application of the results. The total number of particular statements is, however, too large to be covered completely. Sometimes, the solutions are rather bulky but can be efficiently obtained with symbolic computation programs.

II. MODEL

The internal flow of a heat-conductive viscous gas is generally described by the boundary problem for the system of conservation equations (mass, momentum, and energy) and an equation of state. No general solution is available in such a statement. High symmetry and relatively low gas velocities reduce the problem complexity, allowing determination of analytical solutions.

A. Problem formulation and model assumptions

The variety of compressible fluid flows is considered to be under the following limitations.

(i) The gas flow field is one dimensional, specified by the only velocity r component.

This can be a flow with the planar symmetry, as in Figs. 1(a) and 1(b), an axisymmetric flow, as in Fig. 1(c), or a centrosymmetric flow, as in Fig. 1(d). The flow domain is limited by two rigid boundaries, generally, in the state of displacement. The boundary $r_1(t)$ is considered to be internal and may physically disappear, being transformed into an element of symmetry at $r_1 = 0$. The boundary $r_2(t)$ is

considered to be external, so that $r_2(t) > r_1(t)$, with t denoting time.

(ii) The gas density ρ is related to the pressure p and the temperature T by the equation of state of the ideal gas:

$$p = \rho R T, \tag{1}$$

where R is the specific gas constant. Other equations of state may be used in this model as well. Some solutions in Sec. III will use the adiabatic law $p/p_0 = (\rho/\rho_0)^\gamma$ as an equation of state, where γ is the specific heat ratio. Index "0" designates the initial value of a variable.

(iii) The gas pressure is spatially uniform, $p = p(t)$, or, in other words, the flow is homobaric. To understand what restrictions this condition imposes on the system properties, we analyze here the momentum equation being nondimensionalized by the scale of the dynamic pressure:

$$\gamma \mathrm{Ma}^2 \widetilde{\rho}\left(\mathrm{Sh}\,\frac{\partial \widetilde{u}}{\partial \widetilde{t}} + \widetilde{u}\frac{\partial \widetilde{u}}{\partial \widetilde{r}}\right) = -\frac{\partial \widetilde{p}}{\partial \widetilde{r}} + \frac{\gamma \mathrm{Ma}^2}{\mathrm{Re}}\left[\frac{4}{3}\frac{1}{\widetilde{r}^n}\frac{\partial}{\partial \widetilde{r}}\left(\widetilde{r}^n \frac{\partial \widetilde{u}}{\partial \widetilde{r}}\right) - n\frac{\widetilde{u}}{\widetilde{r}^2}\right]. \tag{2}$$

Each variable φ in Eq. (2) is nondimensionalized as $\widetilde{\varphi} = \varphi/\overline{\varphi}$, where $\overline{\varphi}$ is the variable scale. Thus, all the terms have order of unity, except dimensionless multipliers Re, Ma, and Sh. In Eq. (2), $\mathrm{Ma} = \overline{u}/c$ is the Mach number, with $c = \sqrt{\gamma R \overline{T}}$ being the sound velocity, $\mathrm{Sh} = L/\overline{u}t$ is the Strouhal number, $\mathrm{Re} = \overline{\rho u} L/\eta$ is the Reynolds number, u is the gas velocity, L is the domain dimension, and η is the gas viscosity. In Eq. (2) and hereafter, the exponent n denotes the flow symmetry: $n = 0$ for planar, $n = 1$ for axial, and $n = 2$ for central symmetry.

It is clear from Eq. (2) that the pressure gradient becomes small at three simultaneous conditions: $\mathrm{Ma}^2 \ll 1$, $\mathrm{Ma}^2\mathrm{Sh} \ll 1$, and $\mathrm{Ma}^2/\mathrm{Re} \ll 1$. For the first condition, we postulate $\mathrm{Ma} \ll 1$. The second condition can be rewritten as $\mathrm{Ma}L/ct \ll 1$. Because the time resolution we are interested in is much rougher than acoustic time L/c, the second condition is always fulfilled. The validity of the third condition can be shown using the kinetic theory of gases, which gives the following expression for the gas viscosity:

$$\eta = \frac{\overline{\rho} v_m l}{3}, \tag{3}$$

where l is the mean free path in the gas, and the mean velocity of the gas molecules v_m can be expressed through the sound velocity c as $v_m = c\sqrt{3/\gamma}$. Then, the Reynolds number can be rewritten as

$$\mathrm{Re} = \frac{\overline{\rho u} L}{\eta} = \sqrt{\frac{\gamma}{3}}\frac{\overline{u} L}{c l} = \sqrt{\frac{\gamma}{3}}\frac{\mathrm{Ma}}{\mathrm{Kn}}, \tag{4}$$

where $\mathrm{Kn} = l/L$ is the Knudsen number.

Keeping in mind the condition $\mathrm{Ma} \ll 1$, we see that the multiplier $\mathrm{Ma}^2/\mathrm{Re} \approx \mathrm{Ma} \times \mathrm{Kn}$ in the square-bracketed term of Eq. (2) is small at $\mathrm{Kn} \ll 1$. In this study, we work with the basic continuous media approach, which demands $\mathrm{Kn} \ll 1$.

Omitting in Eq. (2) all the negligible terms, we have $\partial p/\partial r = 0$, stated in assumption (iii). The homobaric approximation automatically filters out the sound propagation phenomena from the solution. The medium in the model is homogeneous (i.e., the influence of relative motion of medium phases or gas components is negligible).

(iv) The energy balance in the gas is described by the heat equation

$$\rho c_p \frac{\partial T}{\partial t} = \frac{\lambda}{r^n}\frac{\partial}{\partial r}\left(r^n \frac{\partial T}{\partial r}\right) + Q, \tag{5}$$

where c_p is the isobaric specific heat, and λ is the thermal conductivity. The heat production rate $Q(r,t)$ may include homogeneous and heterogeneous components: the first, as a result of chemical reactions between gas species and energy absorption from the illumination, and the second, as a result of all heat and mass transfer processes on the eventual small solid and liquid particles suspended in the gas.

Equation (5) follows from the comparison of different process contributions in the heat balance. For this, we nondimensionalize the energy equation, scaling it by the conductive term, the first item on the right-hand side

$$\widetilde{\rho}\left(\frac{1}{\mathrm{Fo}}\frac{\partial \widetilde{T}}{\partial \widetilde{t}} + \mathrm{Pe}\,\widetilde{u}\frac{\partial \widetilde{T}}{\partial \widetilde{r}}\right) = \frac{1}{\widetilde{r}^n}\frac{\partial}{\partial \widetilde{r}}\left(\widetilde{r}^n \frac{\partial \widetilde{T}}{\partial \widetilde{r}}\right) + \frac{1}{\mathrm{Fo}}\frac{\gamma - 1}{\gamma}\frac{d\widetilde{p}}{d\widetilde{t}} + \mathrm{Pr}\,\mathrm{Ma}^2(\gamma - 1)\left(\frac{\partial \widetilde{u}}{\partial \widetilde{r}}\right)^2 + \frac{\overline{Q} L^2}{\lambda \overline{T}}\widetilde{Q}, \tag{6}$$

where $\mathrm{Pe} = \overline{u} L/\chi$ is the Peclet number, $\mathrm{Pr} = c_p \eta/\lambda$ is the Prandtl number, $\mathrm{Fo} = \chi \overline{t}/L^2$ is the Fourier number, and $\chi = \lambda/\overline{\rho} c_p$ is the heat diffusivity.

The proposed model deals with the processes for which heat transfer due to advection [second term on the left-hand side of Eq. (6)] is negligible in comparison with heat conduction. In [10], it was shown that in the particular case of thermally driven flows, the advective heat propagation can be ignored when

$$\beta \Delta T \ll 1, \quad \beta = \overline{\rho}\left(\frac{\partial}{\partial T}\frac{1}{\rho}\right)_p, \tag{7}$$

where β is the thermal expansion coefficient of the medium and ΔT is the reference temperature difference across the domain. Additionally, the validity of this important limitation is proven *a posteriori* in Sec. IV by direct comparison of analytical solutions of the current model with the results of the full-scale numerical simulation.

The term with the pressure time derivative in Eq. (6) is only important at low Fourier number. In [10], it is shown that for flows driven by temperature variation, the pressure variation in the heat balance can be neglected if

$$\frac{(\gamma - 1)L^2}{\beta \overline{T} \lambda \Delta T V}\left(\overline{Q} + \int_S q_n d\sigma\right) \ll 1, \tag{8}$$

where V is the domain volume, and the integral in the parentheses designates the total heat flux through the boundaries.

The pressure time derivative in Eq. (6) can be expressed through the temperature using the general solution (12) for the pressure obtained in the next section. This substitution reduces Eq. (6) to an independent partial integrodifferential equation with a single dependent variable T. The third term on the right-hand side of Eq. (6) is responsible for the viscous dissipation. It is negligible in comparison with the heat conduction term

because $\mathrm{Ma}^2 \ll 1$ according to the homobaricity condition, and $\mathrm{Pr} \cong 1$ for gases.

We distinguish essentially unsteady cases characterized by low Fourier number $\mathrm{Fo} \lesssim 1$ and quasistatic cases $\mathrm{Fo} \gg 1$ characterized by relatively quick heat propagation when the final temperature profile is formed nearly instantaneously as a function of time-dependent boundary conditions. At high Fourier number (i.e., for quasistatic cases), Eq. (5) reduces to the Poisson equation

$$\frac{\lambda}{r^n}\frac{\partial}{\partial r}\left(r^n\frac{\partial T}{\partial r}\right) = -Q. \tag{9}$$

To complete the problem statement, we specify the boundary conditions for each particular solution in this paper. The boundary conditions can be expressed through the temperature or the heat flux, can depend on time, and can be posed on moving boundaries. In the unsteady case, we should add the initial condition $T(r,0) = T_0(r)$ to close the problem.

The temperature profile in the gas is thus defined solely by the linear equation of heat conduction (5) or (9), boundary conditions, and eventual initial condition. The solution of the energy equation is thus independent from the momentum equation. The fluid motion is driven by relatively slow variation of its density $\rho(r,t)$ due to heat and matter sources, and displacement of the boundaries, and is defined fully by the continuity and heat equations.

B. General solution and its properties

Gas density variation in time is the characteristic feature of the processes studied in this paper. It may be a result of the temperature profile variation from boundary and/or volumetric heat sources, of the boundary motion, of matter production on the boundaries, and in the volume of the domain. From the conservation law, the whole mass of the gas within the boundaries is equal to the initial gas mass plus the mass produced by the matter sources during time interval 0 to t:

$$\int_{r_1(t)}^{r_2(t)} \rho(\xi,t)\,\xi^n d\xi = \int_{r_1(0)}^{r_2(0)} \rho(\xi,0)\,\xi^n d\xi + \int_0^t S(\tau)d\tau, \tag{10}$$

where $\rho(r,t)$ is the gas density. Both sides of Eq. (10) are divided by a constant geometrical multiplier from integration by the rest dimensions.

The system under consideration may be thermodynamically open. Generally, it includes the heat $\mathbf{q}_1(t),\mathbf{q}_2(t)$ and matter $\mathbf{j}_1(t),\mathbf{j}_2(t)$ fluxes through the boundaries as well as the volumetric heat $Q(r,t)$ and matter $J(r,t)$ sources due to chemical reactions, phase transition, radiation sources, etc. The gas may contain a dispersed second phase in the form of droplets or solid particles that may influence the temperature profile between the boundaries as well as the gas production intensity. Space distribution of the second phase should not necessarily be uniform, and external agents such as irradiation may modulate the temperature profile and gas production intensity.

The function representing the cumulative matter source intensity in Eq. (10) is

$$S(t) = \int_{r_1(t)}^{r_2(t)} J(\xi,t)\,\xi^n d\xi + r_1^n j_1(t) - r_2^n j_2(t), \tag{11}$$

where j_i are projections of the fluxes $\mathbf{j}_i$ on the r axis.

We suppose here that the initial pressure p_0 and the initial temperature distribution $T_0(r)$ are known parameters. Combining Eqs. (1) and (10) and assumption (iii), we get the pressure at arbitrary time $t \geq 0$:

$$p(t) = \frac{p_0}{\int_{r_1(t)}^{r_2(t)} \frac{\xi^n d\xi}{T(\xi,t)}}\left[\int_{r_1(0)}^{r_2(0)} \frac{\xi^n d\xi}{T_0(\xi)} + \frac{R}{p_0}\int_0^t S(\tau)d\tau\right]. \tag{12}$$

The concept of finding the fluid velocity field $u(r,t)$ is based on the following. To define the local gas velocity u at a distance r, we apply the mass conservation law for a gas volume between one of the boundaries and the virtual surface at the distance r. The local gas velocity u thus coincides with the velocity of the virtual surface $\dot{r}$. Hereafter, the dot above a function of time denotes the time derivation.

From the conservation law, the mass variation rate in an arbitrary gas volume $[r_1,r]$ is

$$\frac{d}{dt}\int_{r_1(t)}^{r} \rho(\xi,t)\,\xi^n d\xi = \int_{r_1(t)}^{r} J(\xi,t)\,\xi^n d\xi + r_1^n j_1(t). \tag{13}$$

The Leibniz rule for the derivative gives

$$\int_{r_1(t)}^{r} \frac{\partial \rho}{\partial t}\,\xi^n d\xi + r^n\rho u - r_1^n \rho(r_1,t)\dot{r}_1 = \int_{r_1(t)}^{r} J(\xi,t)\,\xi^n d\xi + r_1^n j_1(t), \tag{14}$$

where the velocity of the virtual surface $r(t)$ coincides with the local gas velocity $u(r,t) \equiv \dot{r}(t)$. From Eq. (14), the velocity is

$$u(r,t) = \frac{1}{r^n\rho(r,t)}\left\{r_1^n[\rho(r_1,t)\dot{r}_1 + j_1(t)] + \int_{r_1(t)}^{r} J(\xi,t)\,\xi^n d\xi - \int_{r_1(t)}^{r} \frac{\partial \rho}{\partial t}\,\xi^n d\xi\right\}. \tag{15}$$

Typically, we will omit arguments in $u(r,t) = u$, $T_1(r,t) = T_1$, $I_t(r,t) = I_t$, etc., only retaining them when we need to stress their meaning. Targeting a concise form of presentation, we introduce the following notation:

$$I(r,t) \equiv \int_{r_1(t)}^{r} \frac{\xi^n d\xi}{T(\xi,t)}, \tag{16a}$$

$$I_t(r,t) \equiv \int_{r_1(t)}^{r} \frac{\partial T}{\partial t}\frac{\xi^n d\xi}{T^2(\xi,t)}, \tag{16b}$$

$$I_J(r,t) \equiv \int_{r_1(t)}^{r} J(\xi,t)\,\xi^n d\xi. \tag{16c}$$

From Eqs. (1) and (15) follows the basic expression for the gas velocity:

$$u = \frac{T}{T_1}\left(\frac{r_1}{r}\right)^n \dot{r}_1 + \frac{T}{r^n}\left[I_t + \frac{R}{p}\left(r_1^n j_1 + I_J\right) - \frac{\dot{p}}{p}I\right], \tag{17}$$

where we have chosen the volume of mass conservation between the first boundary $r_1(t)$ and the imaginary moving

surface with coordinate r. When the second boundary $r = r_2(t)$ is taken as a reference, the gas velocity is

$$u = \frac{T}{T_2}\left(\frac{r_2}{r}\right)^n \dot{r}_2 + \frac{T}{r^n}\left\{ I_t - I_t(r_2,t) + \frac{R}{p}[I_J - I_J(r_2,t) - r_2^n j_2] + \frac{\dot{p}}{p} I \right\}. \quad (18)$$

Velocity values calculated from Eqs. (17) and (18) are identical, and it is a matter of convenience to choose either (17) or (18) depending on a particular task. We will refer only to Eq. (17) unless otherwise stated. It is important to note that limitations (i–iv) should be valid in the volume, to which the mass conservation law is applied. Away from the reference volume, the model limitations may be violated.

Knowing the current pressure value $p(t)$ is important for the cases with boundary and volume gas sources; otherwise, we need to know the ratio $\dot{p}/p$ in Eq. (17). It may happen that the pressure is known *a priori*, and there is no need, or it is simply impossible, to evaluate pressure from Eq. (12). In particular, it is the situation when all the processes occur in the internal region, which is much smaller than the outer part. Whatever happens in the internal region only negligibly affects the total pressure, which may be considered as constant. As a result, the pressure-dependent second term in square brackets in Eq. (17) disappears, which simplifies the calculation. It may be the case that the pressure is externally regulated, for example, by some moving parts of the outer boundary or by the gas pressure controllers being limited in space inlet and outlet areas. The velocity calculation approach may still be applied unless the limitations (i–iv) are not violated in the region between r_1 and r.

In spite of the fact that the pressure in our approach is considered to be uniform, it has the same importance as the other terms in Eq. (17) when it is time dependent. It is easy to illustrate, assuming that the boundary r_1 does not move, the temperature is constant, and there are no gas sources at r_1 and in the volume between r_1 and r. From (17), we obtain time- and space-dependent gas velocity defined solely by the uniform pressure variation:

$$u = -\frac{1}{r^n}\frac{\dot{p}}{p}\int_{r_1}^{r} \xi^n d\xi = -\frac{r^{n+1} - r_1^{n+1}}{(n+1)r^n}\frac{\dot{p}}{p}. \quad (19)$$

Equating velocity in Eq. (17) to zero, we obtain conditions allowing the gas to remain at rest at a distance r. In particular, for a time-varying temperature profile $T(r,t)$ and in the absence of mass sources, the pressure should be regulated according to the following condition:

$$p = p_0 \exp\left[\int_0^t \frac{I_t(r,\tau)}{I(r,\tau)} d\tau\right]. \quad (20)$$

The flow profile arising from the boundary mass source may be completely leveled by imposing boundary motion according to

$$r_i = -R\int_0^t \frac{T_i(\tau) j_i(\tau) d\tau}{p(\tau)}, \qquad i = 1,2. \quad (21)$$

The pressure-dependent term $\dot{p}/p$ in Eq. (17) will now be defined through the parameters of the system in the whole domain $[r_1,r_2]$. It may be defined directly using the expression for the pressure (12) or by isolating $\dot{p}/p$ from two expressions, (17) and (18). The general solution for the velocity $u(r,t)$ representing explicitly all the sources of gas motion is

$$u = \frac{T}{r^n}\left\{ \frac{r_1^n}{T_1}\dot{r}_1 + I_t + \frac{R}{p}\left(r_1^n j_1 + I_J\right) - \left[\frac{r_1^n}{T_1}\dot{r}_1 - \frac{r_2^n}{T_2}\dot{r}_2 + I_t(r_2,t) + \frac{RS}{p}\right]\frac{I}{I(r_2,t)}\right\}, \quad (22)$$

i.e., the gas motion as a result of the displacement of the two boundaries, the temperature variation and gas sources on both boundaries, and the volumetric gas production.

The first four terms in expression (22) define the input of all the sources of gas motion between the reference boundary and the imaginary moving surface with coordinate r. Last three terms in the square brackets represent the influence of the pressure variation $\dot{p}/p$ in the whole region. Below, the gas velocity is subdivided into three constituents to highlight the influence of particular gas motion sources:

$$u = u_B + u_T + u_J = \frac{T}{T_1}\left(\frac{r_1}{r}\right)^n (1-A)U_1 + \frac{T}{T_2}\left(\frac{r_2}{r}\right)^n AU_2 + \frac{T}{r^n}[I_t - AI_t(r_2,t)] + \frac{RT}{pr^n}[I_J - AI_J(r_2,t)]. \quad (23)$$

The ratio

$$A(r,t) = \frac{I(r,t)}{I(r_2,t)} = \int_{r_1}^{r} \frac{\xi^n d\xi}{T(\xi,t)} \Big/ \int_{r_1}^{r_2} \frac{\xi^n d\xi}{T(\xi,t)} \quad (24)$$

can be interpreted as a geometrical factor depending on the position of the radius vector between the boundaries: $0 \leqslant A(r,t) \leqslant 1$, becoming zero at $r = r_1$ and unity at $r = r_2$. The geometrical factor $A(r,t)$ acquires a simple form for the uniform temperature profile

$$A = \frac{r^{n+1} - r_1^{n+1}}{r_2^{n+1} - r_1^{n+1}}. \quad (25)$$

The velocities U_i combine the influence of the boundary motion and the presence of the interfacial mass sources:

$$U_1 = \dot{r}_1 + \frac{RT_1}{p} j_1, \quad U_2 = \dot{r}_2 - \frac{RT_2}{p} j_2. \quad (26)$$

From Eqs. (16) and (23) follows that the "thermal" constituent of the velocity u_T vanishes if the temperature is uniform, even if it varies in time $[T = T(t)]$. Similarly, the "mass source" constituent u_J vanishes in the case of a uniform distributed source $[J = J(t)]$.

The cross influence of the motion sources is clearly seen from Eq. (23). Each of three velocity constituents becomes zero when its corresponding source is not active, but all of them contain implicit dependence on the other active sources. Indeed, according to Eq. (12), displacement of boundaries and mass sources varies the pressure, being a part of the expressions for the constituents u_B and u_J. Temporal variation of the temperature profile modifies the geometric factor A because it is a part of all the constituents in the general expression. However, the cross influence typically is relatively weak.

Gas velocity, defined in different ways in Eqs. (17), (18), (22), and (23), can easily be calculated numerically and in many particular cases analytically. However, the analytical

solutions are often quite bulky because of the temperature in the denominator under the integral sign. For the cases when the maximal deviation of the temperature is smaller than the absolute temperatures on the boundaries, we found it practical to decompose into series the inversed temperature and the square of the inversed temperature. First, we introduce the reference temperature, for example $\overline{T} = (T_1 + T_2)/2$, which is an average of the current temperatures on the boundaries. The small parameter is then the relative deviation of the local temperature from the reference temperature

$$\alpha = \frac{T - \overline{T}}{\overline{T}}. \tag{27}$$

Retaining first-order terms in the decompositions, we obtain

$$\frac{1}{T} \approx \frac{1}{\overline{T}}(1 - \alpha + \cdots) = \frac{1}{\overline{T}} - \frac{T - \overline{T}}{\overline{T}^2} + \cdots, \tag{28a}$$

$$\frac{1}{T^2} \approx \frac{1}{\overline{T}^2}(1 - 2\alpha + \cdots) = \frac{1}{\overline{T}^2} - 2\frac{T - \overline{T}}{\overline{T}^3} + \cdots. \tag{28b}$$

The decompositions of (28), containing the temperature only in the numerators, are used in the integrals (16), while everywhere else we use the exact temperature values and profiles known from the heat equation (5). This approximation often gives accurate results, even in the cases when the temperature variation span becomes comparable to the reference temperatures. In most practical cases, it is sufficient to use the 0th approximation [just the first terms in the right parts of Eq. (28)], which we will use below and will refer to as a uniform inversed temperature approximation (UIT):

$$\begin{aligned} &T = \overline{T}(t), && \text{for } T \text{ in denominators in integrals} \\ &T = T(r,t), && \text{elsewhere.} \end{aligned} \tag{29}$$

This works surprisingly well. In the example calculations of Sec. III, this zero-order approximation provides maximum relative velocity deviation from the exact solution of less than α. For the best accuracy, the uniform temperature $\overline{T}(t)$ should be chosen as most representative for the area with the highest rate of density variation.

The geometrical factor A in the UIT approximation becomes the same as defined in Eq. (25) for the uniform temperature profile, and the thermal gas velocity constituent in Eq. (23) transforms into an expression much more convenient for analytics:

$$u_T \approx \frac{1}{r^n}\frac{T}{\overline{T}^2}\left(\int_{r_1}^{r} \frac{\partial T}{\partial t}\xi^n d\xi + \frac{r^{n+1} - r_1^{n+1}}{r_2^{n+1} - r_1^{n+1}}\int_{r_1}^{r_2} \frac{\partial T}{\partial t}\,\xi^n d\xi\right). \tag{30}$$

UIT approximation gives the following simple estimation of pressure:

$$p \approx p_0 \frac{\overline{T}}{\overline{T}_0} + \frac{n+1}{r_2^{n+1} - r_1^{n+1}} R\overline{T}\int_0^t S(\tau)d\tau. \tag{31}$$

One of the main utilities of the UIT approximation comes from the fact that virtually all of the particular exact solutions for gas velocity contain the $T_2 - T_1$ term in the denominator that produces a singularity at equal boundary temperatures. The limit of the exact solutions at $T_1 \to T_2$ is bounded, and it coincides with the solution in the UIT approximation.

When the main sources of the gas motion are concentrated near one of the boundaries, say, boundary one, the gas velocity from the Taylor decomposition of Eq. (17) is

$$u(r_1 + \Delta r) \approx U_1 + \Delta r\left[\frac{\dot{r}_1}{T_1}\frac{\partial T}{\partial r}\bigg|_{r_1} - n\frac{\dot{r}_1}{r_1} + \frac{\partial T/\partial t}{T} - \frac{\dot{p}}{p} + \frac{RT}{p}\left(J_1 - \frac{nj_1}{r_1^n}\right)\right]. \tag{32}$$

This expression excludes calculating the integrals. It is particularly useful when $(r - r_1) \ll L$ so that the term $\dot{p}/p$ may be neglected. Note that the result depends on the dimensionality factor n.

For a thin space between the two boundaries, the gas velocity in axisymmetric and centrosymmetric cases ($n = 1$ or 2) becomes similar to that for the one-dimensional symmetry ($n = 0$). When the distance between the two boundaries is much less than the wall radii ($L \ll r_i$), we substitute self-standing r, r_2, and ξ by r_1. At the same time, we should retain r in the integral limits and in $T = T(r,t)$ as well as ξ in all the terms of the type $T(r,t)$ and $J(r,t)$ under the integral sign because they may vary substantially within the slot. Independently of the dimensionality factor n, the velocity expression in Eq. (17) is thus reduced to

$$\begin{aligned} u &\approx \frac{T}{T_1}\dot{r}_1 + T\int_{r_1}^{r}\left(\frac{1}{T}\frac{\partial T}{\partial t} - \frac{\dot{p}}{p}\right)\frac{d\xi}{T} + \frac{RT}{p}\left(j_1 + \int_{r_1}^{r} J\,d\xi\right) \\ &= \frac{T}{T_1}(1 - A)U_1 + \frac{T}{T_2}AU_2 \\ &\quad + T\left(\int_{r_1}^{r}\frac{\partial T}{\partial t}\frac{d\xi}{T^2} - A\int_{r_1}^{r_2}\frac{\partial T}{\partial t}\frac{d\xi}{T^2}\right) \\ &\quad + \frac{RT}{p}\left(\int_{r_1}^{r} J\,d\xi - A\int_{r_1}^{r_2} J\,d\xi\right) \end{aligned} \tag{33}$$

with the geometrical factor A:

$$A(r,t) = \left(\int_{r_1}^{r_2}\frac{d\xi}{T}\right)^{-1}\int_{r_1}^{r}\frac{d\xi}{T}. \tag{34}$$

Concluding the model section, it is important to make a note about proceeding from the general solution to the analytical solution of a particular task. The current model includes a set of gas motion sources and three possible dimensionalities. Various combinations result in nearly 500 particular tasks in quasisteady case (large Fourier number) and a similar quantity for small Fourier number. Additionally, for the sources, one should define particular temporal functions, so that the overall variety of the particular cases becomes overwhelmingly wide. Therefore, in the following section, we focus on a set of representative particular tasks, demonstrating exact and approximate analytical solutions along with numerical results and comparative analysis aimed at defining typical characteristics of one-dimensional homobaric gas flows.

III. PARTICULAR CASES

In this section of the paper, we find solutions for gas flows generated by each possible motion source and for various combinations of them, introducing particular dependencies $\dot{r}_i(t)$, $T_i(t)$, $J(t)$, and $j_i(t)$ in the general solution. The major aspect of the analysis is related to the thermally driven flows that we estimate as most frequent. We limit the variety of the thermal tasks by the quasistatic heat equation (9), which corresponds to high Fourier number.

As an example of real-life conditions when the quasisteady approach is accurate, we can discuss the experiment for simulation of astrophysical dust clouds [36] in a chamber with heating elements placed at a distance 4 cm in the chamber, which is filled by air with pressure 30 Pa at room temperature. The frequency of the temperature variations was 2 Hz. For the above mentioned conditions, the Fourier number is Fo ≈ 23, which is sufficient to use the quasistatic approximation.

In all the considered cases, the exact analytical solutions and their approximations are obtained. In all the cases, the presence of both boundaries and particular conditions on them are essential for the formation of the velocity profiles.

A. Boundary temperature variation

Below, we treat the problems of the gas motion in a domain restricted by two nonmoving boundaries $r_1(t) = r_{10}$, $r_2(t) = r_{20}$, when one or two thermal boundary conditions vary in time. Nonuniformly heated gas starts flowing from regions where local time derivative $\partial T/\partial t$ is positive (higher) when compared to the regions where it is negative (lower). The animation in the Supplemental Material [12] illustrates this explanation with synchronously animated temperature and velocity profiles, along with a velocity vector field.

We use the known solutions of the quasistatic heat equation (9) with the boundary conditions of the first type

$$T(r_1,t) = T_1(t), \quad T(r_2,t) = T_2(t) \tag{35}$$

for all three geometries (planar, axisymmetric, and centrosymmetric) to find the gas velocity and pressure. The expressions for gas velocity and pressure obtained below for the boundary conditions (35) are applicable for any other thermal boundary conditions. For example, in the case of boundary conditions of the second type, say $(\partial T/\partial r)|_{r=r_2} = -q_2(t)/\lambda$, Eq. (9) has the solution

$$T = T_1 - \frac{q_2}{\lambda}(r - r_1), \tag{36}$$

from where $T_2 = T(r_2) = T_1 - q_2 L/\lambda$, which should be used as the temperature on the second boundary in Eq. (35).

Due to the relative simplicity of the quasistatic temperature distribution, it appears possible to obtain exact analytical solutions, when mass sources are absent. Substituting $J(r,t) = 0$, $j_i = 0$, and $\dot{r}_i = 0$ $(i = 1,2)$ in Eqs. (12) and (23), we obtain the gas velocity profile

$$u = u_T = \frac{T}{r^n}\left[I_t - I\,\frac{I_t(r_2,t)}{I(r_2,t)}\right] \tag{37}$$

and the time-dependent pressure

$$p = p_0 \frac{I(r_2,0)}{I(r_2,t)}. \tag{38}$$

The analysis of the gas flow for particular cases is performed for linear or periodic temperature variation in time on the boundaries. The linear temporal profile of temperature variation is convenient to find analytical solutions and for illustrations. In practice, the surface heating is often realized applying constant power of heat production, activated at a given moment. The corresponding temporal profiles are complicated functions, but in the initial interval they are often well described by linear dependence.

The goal of the further analysis is to visualize typical gas velocity profiles, to compare our analytical and approximate solutions with the corresponding numerical simulation in the full Navier-Stokes equation system, to give an idea of what happens when a quasisteady regime is no longer valid (Fo $\lesssim 1$), and to highlight profile peculiarities for different dimensionalities n.

1. *Infinite heated plates ($n = 0$)*

Suppose that the gas fills a gap of width L between parallel solid plates with coordinates r_1 and r_2. The boundary temperatures vary in time as given by functions $T_1(t)$ and $T_2(t)$. This is the classical configuration of measurement cell, which is widely used in experimental studies of heat transfer and transport phenomena. The plate dimensions in reality are finite, but the small distances between them allow the side effect influence in the central part of the cell to be neglected. In the absence of volumetric heat sources ($Q = 0$), the temperature distribution for the quasistationary heat equation (9) in the planar gap $r_1 \leqslant r \leqslant r_2$ is a linear function of the coordinate r:

$$T = \frac{(r - r_1)T_2 + (r_2 - r)T_1}{L}. \tag{39}$$

Knowing the temperature, we can readily obtain the gas pressure from Eqs. (38), (39), and (16a):

$$p = p_0 \frac{\ln(T_{20}/T_{10})}{\ln(T_2/T_1)}\,\frac{T_2 - T_1}{T_{20} - T_{10}}. \tag{40}$$

Hereafter, $T_{10} \equiv T_1(0)$, $T_{20} \equiv T_2(0)$, and p_0 are the boundary temperatures and the pressure at $t = 0$, respectively. If $T_{20} = T_{10}$, then Eq. (40) has a discontinuity which is resolved as

$$p\big|_{T_{10}=T_{20}} = p_0 \frac{T_2 - T_1}{T_{10}\ln(T_2/T_1)}. \tag{41}$$

Upon introducing the normalized dimensionless coordinate fixed on the gap walls as

$$x = \frac{r - r_1}{L}, \quad L = r_2 - r_1, \tag{42}$$

the temperature profile of Eq. (39) transforms into

$$T = x\,T_2 + (1 - x)\,T_1. \tag{43}$$

From Eqs. (43), (16a), (16b), and (37), the gas velocity profile is

$$u = L\left[T\frac{\ln(T/T_1)}{\ln(T_2/T_1)} - xT_2\right]\frac{\dot{T}_2/T_2 - \dot{T}_1/T_1}{T_2 - T_1}. \tag{44}$$

It is important to note that the velocity profile in (44) is scalable by the distance between the boundaries L.

In the UIT approximation, the velocity profile becomes as simple as a parabola with the extremum in the mid-plane

between the plates:

$$u_{\mathrm{UIT}} = \frac{\dot{T}_2 - \dot{T}_1}{2\overline{T}^2} T(x-1)xL, \tag{45}$$

and the pressure obeys the simple isochoric law $p/p_0 = \overline{T}/\overline{T}_0$. The expression for the velocity has a singularity when $T_1 \to T_2$ at $\dot{T}_1 \neq 0$ and/or $\dot{T}_2 \neq 0$. The limit exists and coincides with the UIT approximation (45) with $\overline{T}(t) = T_1 = T_2$.

The profile always has a single extremum located in

$$X = \frac{T_1}{T_2 - T_1}\left[\exp\left(\frac{T_2}{T_2 - T_1}\ln\frac{T_2}{T_1} - 1\right) - 1\right]. \tag{46}$$

For $T_1 \to T_2$, the velocity extremum is located in the middle of the region: $X = \frac{1}{2}$. At greatly different boundary temperatures, the extremum can be significantly shifted from the middle: $X \to e^{-1}$ at $T_2 \gg T_1$ and $X \to 1 - e^{-1}$ at $T_1 \gg T_2$. The general expression for the extreme velocity remains proportional to L:

$$u(X) = \frac{\dot{T}_2/T_2 - \dot{T}_1/T_1}{T_2 - T_1} T_1 L \times \left[\frac{T_2}{T_2 - T_1} - \exp\left(\frac{T_2}{T_2 - T_1}\ln\frac{T_2}{T_1} - 1\right)\right]. \tag{47}$$

The velocity profiles near the boundaries are well described by linear functions, particularly when the extremum is strongly shifted from the domain center. The velocity slopes on the boundaries are defined by the Taylor decompositions

$$u_i' = \left[\frac{T_2 - T_1}{\ln(T_2/T_1)} - T_{(3-i)}\right]\frac{\dot{T}_2/T_2 - \dot{T}_1/T_1}{T_2 - T_1}, \quad i = 1,2. \tag{48}$$

Below, we analyze the gas flow for a particular case of periodic temperature variation on the left and constant temperature on the right boundary:

$$T_1 = T_0 + \Delta T \sin(\omega t), \quad T_2 = T_0. \tag{49}$$

Dimensionless velocity is introduced as a ratio $\tilde{u} = u/u_{\max}$, where $u_{\max} = L\omega\Theta/8$ is the maximal velocity in time and space obtained from Eq. (47). The velocity profile along coordinate x depends only on two dimensionless parameters: ratio $\Theta = \Delta T/T_0$ and dimensionless time $\tau = \omega t$:

$$\tilde{u} = \frac{8}{\tan\tau}\left\{-\frac{x}{1 + \Theta\sin\tau} + \left(x - 1 - \frac{x}{1 + \Theta\sin\tau}\right) \times \frac{\ln[1 - x + x/(1 + \Theta\sin\tau)]}{\ln(1 + \Theta\sin\tau)}\right\}. \tag{50}$$

For a quantitative treatment, we took relative temperature variation $\Theta = 0.2$. Figure 2(a) shows velocity profiles in a quasistationary gas flow regime. At the time instants $\tau = i\pi$, $i \in \mathbb{Z}$, all the profiles coincide. At given Θ, no visible difference is seen between the exact solution and the first-order approximation (28). Even zero-order UIT approximation (29) deviates from the exact solutions at particular time instants with maximal relative values of less than 0.15. It should be considered as a good approximation in view of the rather large temperature variation $\Theta = 0.2$. See Supplemental Material [12] for animated solution of the gas flow in a planar gap.

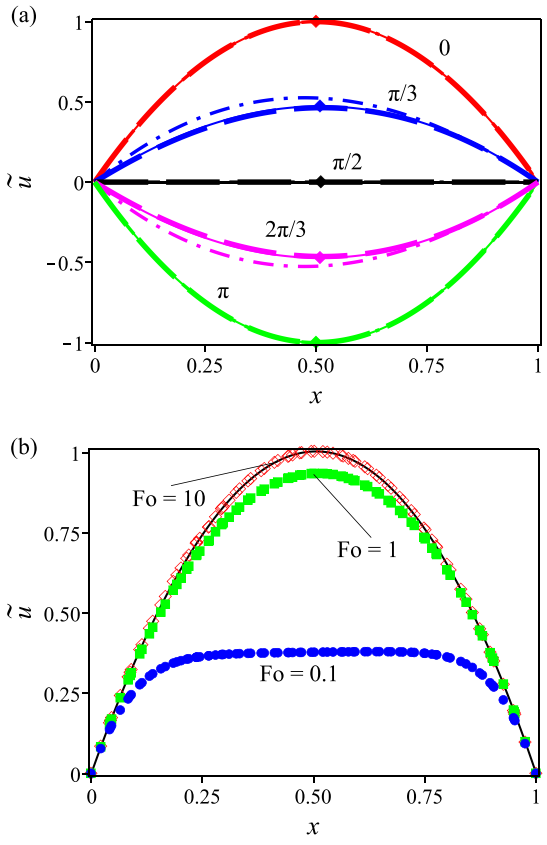

FIG. 2. Flow between two heating plates: (a) Dimensionless velocity profiles for boundary conditions (49) with $\Theta = \Delta T/T_0 = 0.2$: the exact analytic solution (50) (thin solid lines), the UIT approximation (dashed-dotted lines), and the first-order approximation (28) (thick dashed lines) at several time instants (numbers near the curves show the ωt value). The diamonds locate the velocity extrema. (b) Comparison of the analytical solution (52) (solid line) and three numerical solutions (red diamonds Fo = 10, green squares Fo = 1, and blue circles Fo = 0.1) for boundary conditions (51) at the time instant $\tau = kt/T_0 = \frac{1}{15}$.

Figure 2(b) illustrates what occurs upon transition from the quasistationary to the nonstationary regime of flow. The velocity profiles are presented for antisymmetric linear temperature variation on both boundaries

$$T_1 = T_0 + k\,t, \quad T_2 = T_0 - k\,t. \tag{51}$$

The velocity is normalized by $u_{\max} = kL/4T_0$, which corresponds to $u(X)$ at $t = 0$. After normalization, the velocity is completely defined only by dimensionless coordinate (42) and dimensionless time $\tau = kt/T_0$:

$$\tilde{u} = \frac{4}{\tau(1-\tau)}\left\{-\frac{1-\tau}{1+\tau}x + \left(1 - \frac{2\tau}{1+\tau}x\right) \times \frac{\ln[1 - 2x\tau/(1+\tau)]}{\ln[(1-\tau)/(1+\tau)]}\right\}. \tag{52}$$

The solution is defined at $\tau < 1$ because T_2 becomes zero at $\tau = 1$, and the velocity tends to infinity.

The CFD numerical full-scale simulations were conducted using the ANSYS FLUENT software with the mesh generated in

GMSH software [38]. The simulation is performed for a set of values of the Fourier number defined as $\mathrm{Fo} = \chi T_0/kL^2$.

The graphs clearly show that the numerical and analytical solutions coincide when the model requirement on high Fourier number is fulfilled ($\mathrm{Fo} = 10$). The maximal relative deviation of the velocity calculated at $\mathrm{Fo} = 1$ is less than 0.07, but it is already more than 0.5 at $\mathrm{Fo} = 0.1$. The velocity maximum slightly moves from its central position at $\mathrm{Fo} = 10$ toward the right wall for smaller Fo when $\tau \to 1$. The formation of a flat zone in the central part is a typical property of essentially nonstationary flows in the current example.

2. *Two coaxial infinite cylinders ($n = 1$)*

For an annular gap ($n = 1$) between two infinitely long cylinders, the solution of Eq. (9) with boundary conditions (35) is

$$T = T_1 + (T_2 - T_1)\frac{\ln y}{\ln G}, \tag{53}$$

where the dimensionless coordinate y is linearly related to x from Eq. (42):

$$y = r/r_1 = 1 + (G-1)x. \tag{54}$$

New dimensionless coordinate y makes the expressions shorter. The "tube-in tube" configuration is common for heat exchangers and chemical reactors.

Solutions in nonplanar geometries ($n > 0$) contain a new parameter: a ratio of external and internal radii

$$G = \frac{r_2}{r_1}. \tag{55}$$

As with the previous task, all the solutions can be extended on any type of thermal boundary conditions, replacing T_i by $T(r_i,t)$ from redefined boundary conditions.

Explicit expressions for pressure and velocity through the boundary conditions follow from Eqs. (38) and (37) as

$$p = p_0\frac{T_2 - T_1}{T_{20} - T_{10}}\frac{E(G,0) - E(1,0)}{E(G,t) - E(1,t)} \times \exp\left[2\left(\frac{T_1}{T_2 - T_1} - \frac{T_{10}}{T_{20} - T_{10}}\right)\ln G\right], \tag{56}$$

$$u = \frac{\dot T_2/T_2 - \dot T_1/T_1}{(T_2 - T_1)^2}\frac{L\ln G}{[E(G,t) - E(1,t)](G-1)y} \times [E(y,t)(G^2T_1 - T_2)T + E(1,t)(y^2T_2 - G^2T)T_1 - E(G,t)\left(y^2T_1 - T\right)T_2], \tag{57}$$

where $L = r_2 - r_1$ and $E(y,t) = \mathrm{Ei}[\frac{2T(y,t)}{T_1(t) - T_2(t)}\ln G]$, with Ei being the exponential integral function of the real argument.

The UIT approximation from Eq. (30) gives a simple expression

$$u_{\mathrm{UIT}} = \frac{\dot T_2 - \dot T_1}{2\overline{T}^2}\frac{LT}{(G-1)y}\left[\frac{G^2}{G^2-1}(1 - y^2) + y^2\frac{\ln y}{\ln G}\right] \tag{58}$$

that coincides with the limit of Eq. (57) in the singularity case when $T_1 \to T_2$ at $\dot T_1 \neq 0$ and/or $\dot T_2 \neq 0$. The velocity

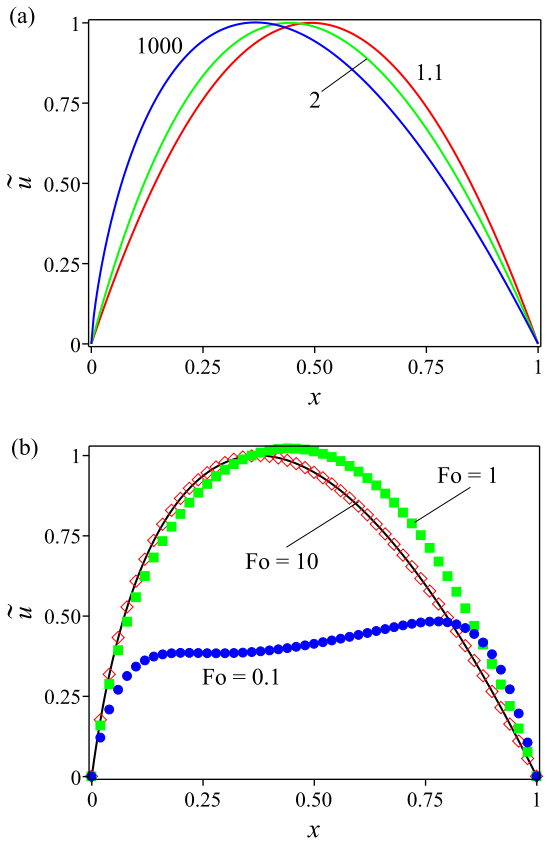

FIG. 3. Flow between two heating cylinders: (a) Profiles of dimensionless velocity at several values of the ratio $G = r_2/r_1$ (numbers near the curves). The profiles are calculated at $t = 0$ for the periodic boundary conditions (49) with $\Theta = \Delta T/T_0 = 0.2$. (b) Comparison of the analytical (solid line) and three numerical solutions (red diamonds $\mathrm{Fo} = 10$, green squares $\mathrm{Fo} = 1$, and blue circles $\mathrm{Fo} = 0.1$) in the case of linear boundary conditions (51) at $\tau = kt/T_0 = \frac{1}{15}$ and $G = 10$.

extremum and its coordinate in the UIT approximation are

$$u_{\mathrm{UIT}}(X_{\mathrm{UIT}}) = \frac{\dot T_2 - \dot T_1}{2\overline{T}^2}\frac{LT}{G-1}\frac{1 - \Omega(G)}{\sqrt{2\left(G^2-1\right)\Omega(G)\ln G}}, \tag{59}$$

$$X_{\mathrm{UIT}} = \frac{1}{G-1}\left\{\exp\left[\frac{\Omega(G)}{2} + \frac{G^2\ln G}{G^2-1} - 1\right] - 1\right\}, \tag{60}$$

where $\Omega(G) = W_0[\frac{2G^2\ln G}{G^2-1}\exp(2 - \frac{2G^2\ln G}{G^2-1})]$ with W_0 being the single-valued Lambert function. Both formulas give accurate results for not too high values of G. The relative deviation from the exact value is less than 0.15, even for $G \to \infty$.

In the same manner as for the flat geometry, we present in Fig. 3 analysis of the gas flow for two particular types of time-dependent boundary conditions (49) and (51). The velocity is normalized similarly, by Eq. (59). Properties of the velocity profiles are very close to those in the planar case ($n = 0$) as well as the velocity profiles for periodic temperature variation in Fig. 3(a). The latter profiles correspond to three different values of G at the time instant when the temperature time derivative is maximal. Upon growing of G, the velocity

extremum shifts toward the internal boundary r_1, and for $G \to \infty$ the extremum location $X \to 1/e$.

The influence of the transition from quasistationary (Fo $\gg$ 1) to essentially nonstationary (Fo $\ll$ 1) regimes of heat transfer on the velocity profiles is illustrated in Fig. 3(b). The main features are similar to those for the flat geometry ($n = 0$), accounting for the shift of the velocity maximum toward the inner boundary and increasing asymmetry of the profiles at growing G.

3. *Two concentric spheres ($n = 2$)*

For the gas confined between two concentric spheres from Eq. (9) and boundary conditions (35), we obtain the following temperature profile:

$$T = \theta + \frac{\phi}{y}, \quad \theta = \frac{GT_2 - T_1}{G-1}, \quad \phi = \frac{T_1 - T_2}{G-1}, \tag{61}$$

where y is the dimensionless coordinate (54) and G is the ratio of the wall radii defined by Eq. (55).

The auxiliary integrals in Eq. (37) are expressed through θ and ϕ :

$$\begin{aligned} I &= \frac{L^3}{(G-1)^3}\left(\frac{y^3-1}{3\theta} - \phi\frac{y^2-1}{2\theta^2}\right. \\ &\quad \left. +\phi^2\frac{y-1}{\theta^3} - \frac{\phi^3}{\theta^4}\ln\frac{y\theta+\phi}{\theta+\phi}\right), \\ I_t &= \frac{L^3}{(G-1)^3}\left[\frac{\dot\theta}{\theta^2}\frac{y^3-1}{3} + \left(\frac{\dot\phi}{2} - \frac{\phi\dot\theta}{\theta}\right)\frac{y^2-1}{\theta^2}\right. \\ &\quad +\left(\frac{3\phi^2\dot\theta}{\theta} - 2\phi\dot\phi\right)\frac{y-1}{\theta^3} \\ &\quad +\left(\frac{\phi^4\dot\theta}{\theta^4} - \frac{\phi^3\dot\phi}{\theta^3}\right)\frac{y-1}{(y\theta+\phi)(\theta+\phi)} \\ &\quad \left. +\left(\frac{3\phi^2\dot\phi}{\theta^4} - \frac{4\phi^3\dot\phi}{\theta^5}\right)\ln\frac{y\theta+\phi}{\theta+\phi}\right]. \end{aligned} \tag{62}$$

The exact solutions for pressure and velocity follow from Eqs. (38) and (37). The UIT approximations may be expressed in a compact way without θ and ϕ. The pressure is defined by the first term on the right-hand side of Eq. (31), while the velocity is

$$u_{\mathrm{UIT}} = -\frac{\dot T_2 - \dot T_1}{2\overline{T}^2 y^2}\frac{LT}{G-1}\frac{(G-y)(y-1)G[G+(G+1)y]}{G^3-1}. \tag{63}$$

The velocity extremum and its coordinate in the UIT approximation are

$$\begin{aligned} &u_{\mathrm{UIT}}(X_{\mathrm{UIT}}) \\ &= \frac{\dot T_1 - \dot T_2}{2\overline{T}^2}\frac{LT}{G-1}\left[\frac{G}{G-1} - \frac{3G^3}{(G^3-1)\left(\frac{2G^2}{G+1}\right)^{2/3}}\right], \end{aligned} \tag{64}$$

$$X_{\mathrm{UIT}} = \frac{\sqrt[3]{\frac{2G^2}{G+1}} - 1}{G-1}. \tag{65}$$

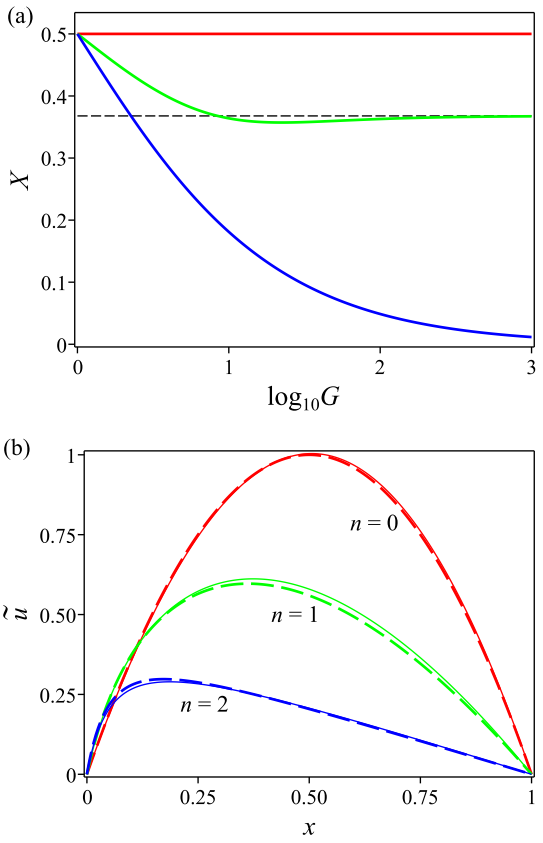

FIG. 4. Boundary temperature variation: (a) Velocity extremum location as a function of decimal logarithm of the ratio $G = r_2/r_1$ in all three geometries for boundary conditions (49) at $\tau = 0$ and fixed r_1. (b) Comparison of the velocity distributions in different symmetries for linear boundary conditions (51) at dimensionless time $\tau = kt/T_0 = \frac{1}{15}$ and $G = 10$. Dashed lines are for the UIT approximation.

Analytical expressions for the gas velocity related to the time-dependent boundary conditions (49) and (51) are not presented here because they are too bulky. The tendencies for the velocity profile transformation are becoming more profound for central symmetry. The shift of the velocity extremum toward the internal boundary is illustrated in Fig. 4.

The higher G becomes, the more the velocity extremum is shifted toward the internal boundary [Fig. 4(a)]. Unlike planar and axisymmetric cases, the velocity extremum in centrosymmetric tasks asymptotically tends to $x = 0$ at $G \to \infty$. Typical velocity profiles for $n = 0,1,2$ at linear temperature variation on the walls (51), dimensionless time $\tau = kt/T_0 = \frac{1}{15}$, and $G = 10$ are presented in Fig. 4(b). The velocity is normalized by the maximal velocity for the planar geometry (47).

The gas velocity profiles always have the same sign in the whole domain for all the flows driven by the time-dependent thermal boundary conditions. In other words, there cannot be stagnant points, except for boundaries. The proof of this statement is based on the general solution for the velocity (22), where the multiplier T/r^n may be omitted as always positive. The velocities are zero on the boundaries. Therefore, to have no sign alteration between the boundaries, the velocity profile should have a single extremum. Taking the space derivative

from the expression in the square brackets in Eq. (37) and equating it to zero, we obtain the equation to find the roots for the extrema of the velocity profiles as $\partial T/\partial t = TC(t)$.

The function $C(t)$ is the ratio of the definite integrals in Eq. (37) and thus does not depend on coordinates. This equation always has only one solution due to monotonicity of the temperature profile between the boundaries [the property of the general solution of Eq. (9)], thus giving the proof for the sole extremum in the whole domain.

B. Moving boundaries and boundary mass sources

Suppose that there are no volumetric sources $[J(r,t) = 0]$ and the temperature is always uniform $(\partial T/\partial r = 0)$ or static $(\partial T/\partial t = 0)$. From Eq. (23), it follows that in both cases, the only source of motion may be related to the boundaries u_B:

$$u = u_B = \frac{T}{T_1}\left(\frac{r_1}{r}\right)^n (1-A)U_1 + \frac{T}{T_2}\left(\frac{r_2}{r}\right)^n AU_2, \tag{66}$$

with the geometric factor A from Eq. (25). We recall that the velocities U_1 and U_2 comprise the velocity of the boundary displacement and the gas velocity on the boundary because of surface mass sources, according to Eq. (26). The two effects are identical for the generation of the gas motion and peculiarities of its pattern (in the case of moving boundaries, instantaneous pattern). The pressure is still defined by the full equation (12).

1. Boundary displacement

Here, we analyze gas flow induced by motion of rigid walls in the absence of any mass and heat sources. Boundary velocity must be much less than the sound propagation velocity $[\dot{r}_i \ll c]$ to meet model assumption (iii). All possible acoustic phenomena are thus filtered out from the solution. The solution gives the velocity "averaged" over multiple "acoustic times."

In the isothermal approximation $T(r,t) = T_0$ and in the absence of mass sources on the boundaries $U_i = \dot{r}_i$, the pressure from Eq. (12) is

$$p = p_0 \frac{r_{20}^{n+1} - r_{10}^{n+1}}{r_2^{n+1} - r_1^{n+1}}, \tag{67}$$

where r_{20} and r_{10} are the boundary coordinates at $t = 0$. For the adiabatic approximation $p/p_0 = (\rho/\rho_0)^\gamma$ in assumption of uniform temperature $T = T(t)$, the pressure is

$$p = p_0 \left(\frac{r_{20}^{n+1} - r_{10}^{n+1}}{r_2^{n+1} - r_1^{n+1}}\right)^\gamma. \tag{68}$$

Gas density in the adiabatic process equals that in the isothermal process, and the gas velocity in both cases is

$$u = \frac{\left(r^{n+1} - r_1^{n+1}\right) r_2^n \dot{r}_2 + \left(r_2^{n+1} - r^{n+1}\right) r_1^n \dot{r}_1}{\left(r_2^{n+1} - r_1^{n+1}\right) r^n}. \tag{69}$$

In the axisymmetric and the centrosymmetric geometries, moving boundaries generate particular components of gas motion. To highlight the peculiarities of this case, we impose an additional requirement, considering that the gas density is constant. The whole volume remains the same, while the boundaries should move as

$$\dot{r}_2 = \left(\frac{r_1}{r_2}\right)^n \dot{r}_1. \tag{70}$$

For the flat geometry, we obtain $\dot{r}_2 = \dot{r}_1$. Obviously, the gas is motionless in a coordinate system that is fixed with one of the boundaries. In axisymmetric and centrosymmetric geometries, the gas does move with respect to each boundary, with the velocity $u = (r_1/r)^n \dot{r}_1$, in spite of the fact that the pressure and gas density are stationary and uniform. The center of gravity of the gas mass evolves as $r_{\text{cgrav}} = [r_2^{n+1} - r_1^{n+1}]^{1/(n+1)}$ in the coordinate system fixed on the element of symmetry.

Below, we combine moving boundaries and quasistationary temperature variation.

2. Moving boundaries with varying temperatures

Consider a planar $(n = 0)$ gas flow generated by heated walls which are in a state of motion. The expression for the pressure comes from Eq. (38):

$$p = p_T \frac{r_{20} - r_{10}}{r_2 - r_1}, \tag{71}$$

where p_T is the solution for nonmoving heated boundaries given by Eq. (40). The resultant velocity can be presented as an algebraic sum from two sources, according to Eq. (23) :

$$u = u_T + \frac{(r_2 - r)\dot{r}_1 + (r - r_1)\dot{r}_2}{r_2 - r_1}, \tag{72}$$

where u_T is the solution for nonmoving heating boundaries from Eq. (44) with r_1 and r_2 replaced by $r_1(t)$ and $r_2(t)$, and t is a parameter.

To give an example of the joint action of the sources, we consider a particular task when the temperature of the left wall has a sinusoidal temporal component, while the wall itself is in antiphase periodic displacement. The right wall stays at rest at a constant temperature:

$$\begin{aligned} &T_1 = T_0 + \Delta T \sin(\omega t), \quad && r_1 = r_{10} - \Delta r \sin(\omega t), \\ &T_2 = T_0, && r_2 = r_{20}. \end{aligned} \tag{73}$$

The following analysis of the velocity profiles is based on UIT approximation; otherwise, the expressions are too bulky. The defining parameters can be reduced to the sine phase ωt and two dimensionless complexes: $\Theta = \Delta T/T_0$, $\delta = \Delta r/(r_{20} - r_{10})$ where δ is the relative wall displacement. In Fig. 5(a), the velocity profiles are presented for $\Theta = \frac{1}{15}$, $\delta = 0.01$, so that the wall velocity and the gas velocity due to thermal expansion are comparable. The velocity is normalized by $u_{\max}$ and plotted versus dimensionless coordinate $x = (r - r_{10})/(r_{20} - r_{10})$. The maximum velocity $u_{\max}$ in time and space is a maximum of the left boundary velocity at $t = 0$: $u_B = \omega \Delta r$ and the velocity at the extremum point at $t = 0$: $u_{\text{extr}} = \omega \Theta \Delta r (2\delta/\Theta - 1)^2/8\delta$.

In Fig. 5(b), one can see how the relation between the relative temperature amplitude Θ and relative boundary displacement δ changes the shape of the velocity profiles: when $\Theta > 2\delta$, the profile has distinct extremum and there is a stagnant point with zero velocity, otherwise the profile is monotonous. Velocity profiles obtained by numerical simulation in ANSYS FLUENT software under an $\text{Fo} \gg 1$ condition

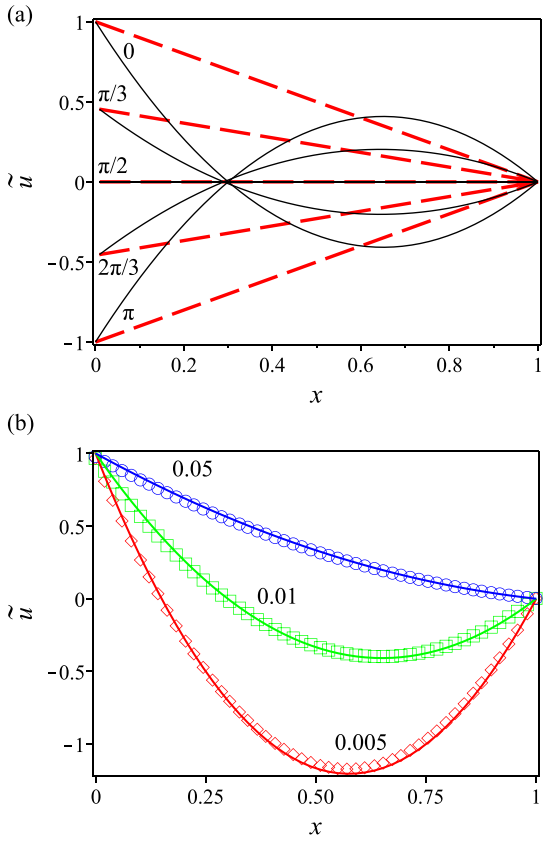

FIG. 5. Heating and moving wall: (a) Analytic profiles (thin solid curves) of dimensionless gas velocity for boundary conditions (73) at $\Theta = \Delta T/T_0 = \frac{1}{15}, \delta = \Delta r/(r_{20} - r_{10}) = 0.01$. Thick dashed lines represent the solution for constant temperature of the left wall $T_1 = T_0$. The numbers next to the curves show corresponding values of ωt. (b) Dimensionless velocity profiles from Eq. (72) (solid curves) and numerical simulation (symbols), at $t = 0$, $\Theta = \frac{1}{15}$, and three values of δ (numbers next to the curves). The profiles are normalized by corresponding wall velocity.

almost coincide (relative error not more than 2.5%) with the analytic profiles.

The results of the analysis may be treated in a way that if the temperature of one of the walls varies in time, it is possible to reduce the induced gas velocity by moving the same wall. The velocity profile will be lower, and there may appear a point with zero velocity. For $\Theta > 2\delta$, the stagnant point $r = r_0$ falls within the domain. The coordinate of the stagnant point for the above mentioned conditions is

$$r_0(t) = r_1(t) + 2(r_{20} - r_{10})\delta/\Theta. \tag{74}$$

The splitting of the solution into two independent terms, similarly to Eqs. (71) and (72), in general is not valid for other geometries, but it gives a good approximation when at least one of the terms is small.

3. *Boundary mass sources*

In this section, we consider gas motion driven by mass sources $j_1(t)$ and $j_2(t)$ on the boundaries in a closed domain with nonmoving boundaries and constant temperature $T(r,t) = T_0$. In this case, the gas velocity is defined by Eq. (66), where $U_i = RT_0 j_i/p$, and the pressure from Eq. (12) is

$$p = p_0 + RT_0 \frac{n+1}{r_2^{n+1} - r_1^{n+1}} \int_0^t \left[r_1^n j_1(\tau) - r_2^n j_2(\tau)\right] d\tau. \tag{75}$$

Such systems happen in cavities with some physicochemical transformations on the walls, such as phase transition, absorption, chemical reaction, etc. Another realization of such a system is related to permeable walls, as shown in Fig. 1(c). For the latter case, we present two particular illustrative cases: (1) stationary gas density in the domain and (2) equal flow densities on both boundaries. For the first case, one may imagine constant overpressure in the region behind the first permeable wall and an open space outside the second, also permeable, wall. The gas flows through the cavity, maintaining constant pressure and thus density in the cavity. The flow densities are related in the same manner as for the moving boundaries (70), i.e., $j_2 = (r_1/r_2)^n j_1$. In this case, the gas pressure is constant ($p = p_0$) and the velocity is

$$u = \frac{RT_0 j_1}{p_0} \frac{1}{y^n}, \tag{76}$$

where y is the dimensionless coordinate (54). The extreme velocity in time and space is $u_{\max} = U_1 = RT_0 j_1/p_0$.

The second case of equal in or out fluxes $j_1 = -j_2 \equiv j_0$ may be illustrated by the cavity bounded by two walls of identical permeability; the pressure outside the cavity, $r < r_1$ and $r > r_2$ is the same but is not equal to the uniform pressure inside the cavity $r_1 < r < r_2$. The velocity from Eq. (66) and the pressure from Eq. (75) are

$$u = \frac{RT_0 j_0}{p} \frac{(G+1)G^n - (G^n+1)y^{n+1}}{(G^{n+1}+1)y^n}, \tag{77}$$

$$p = p_0 + \frac{RT_0 j_0 (n+1)(G-1)}{L} \frac{G^n+1}{G^{n+1}-1} t, \tag{78}$$

where G is the ratio of the wall radii (55). The velocity is maximal at $t = 0$.

The dimensionless velocity profiles corresponding to the illustrative cases mentioned above are presented in Fig. 6. The velocity is normalized by $RT_0 j_0/p(t)$, and it depends only on x defined by Eq. (42) and on G. The calculations are conducted at $G = 5$. At large G for $n > 0$, the dimensionless velocity profile in almost the whole domain is described by linear function with the slope -1 [see dashed curve on Fig. 6(b)]. In the planar case ($n = 0$), the slope is -2. When G tends to unity, the dimensionless velocity profiles at $n > 0$ are identical to that at $n = 0$. The location of the stagnant point (where $u = 0$) is

$$x_0 = \frac{G^n}{G^n+1} \frac{G+1}{G-1} \left(\frac{G^{-n}+1}{G+1}\right)^{\frac{n}{n+1}} - \frac{1}{G-1}. \tag{79}$$

C. Distributed sources

Upon illumination, gas molecules absorb part of the irradiation energy, leading to the variation of the gas temperature and its density. Homogeneous nonuniform chemical reactions have the same effect. Small cloud particles, heated by illumination or changing their temperature due to the phase transition, represent other cases of distributed thermal sources. All of

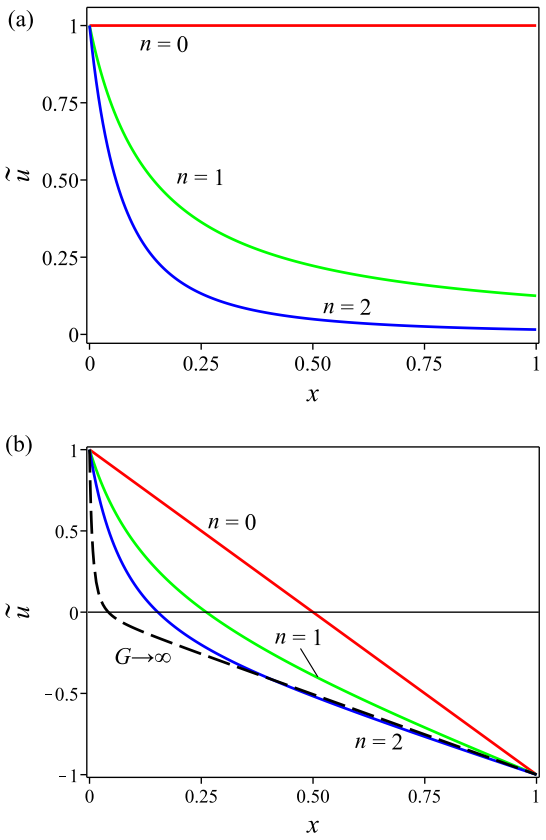

FIG. 6. Boundary mass sources: (a) Velocity profiles at constant gas density, i.e., for boundary fluxes $j_2 = (r_1/r_2)^n j_1$. (b) Profiles for equal inflow and outflow fluxes $j_1 = -j_2 \equiv j_0$. The radii ratio is $G = 5$ everywhere except for the dashed curve in the plot (b).

them are defined by $Q(r,t)$ in our model. Similarly, there may exist distributed mass sources represented by $J(r,t)$. Space nonuniformity may be rather complicated, as consisting of sequential cloud layers of different density variation intensity.

To highlight peculiarities of such systems, in the two following examples we idle all the sources except for homogeneous and heterogeneous (cloud) mass sources with simple profiles of space nonuniformity. The boundaries stay at rest, there are no boundary mass sources, $U_i = 0$, and the gas temperature profile does not vary in time. The gas velocity profile for nonuniform volumetric matter source from Eq. (23) is a function of the coordinate

$$u = \left[I_J - \frac{I_J(r_2,t)}{I(r_2,t)} I \right] \frac{RT}{pr^n} \tag{80}$$

scaled by the linearly growing in time pressure:

$$p = p_0 + R\,\frac{I_J(r_2,t)}{I(r_2,t)}\,t. \tag{81}$$

1. Arrhenius-type kinetics

Here, we analyze gas motion induced solely by the distributed mass source in the planar case $n = 0$. For constant temperatures on both boundaries $T_1(t) = T_1$, $T_2(t) = T_2$, and $T_1 > T_2$ the temperature profile is given by Eq. (39). We assume that the volumetric mass production rate follows the Arrhenius-type kinetics:

$$J(r) = J_0 \exp\left[-\frac{E}{RT(r)} \right]. \tag{82}$$

In spite of the fact that the temperature profile is stationary, the motion does arise because of mass production rate dependence on the nonuniform temperature.

The solutions for the velocity and the pressure are defined by Eqs. (80) and (81) with following integral functions:

$$I_J = \frac{J_0 L}{T_2 - T_1} \left\{ T \exp\left(-\frac{E}{RT} \right) - T_1 \exp\left(-\frac{E}{RT_1} \right) - \left[\mathrm{Ei}\left(\frac{E}{RT} \right) - \mathrm{Ei}\left(\frac{E}{RT_1} \right) \right] \frac{E}{R} \right\}, \tag{83}$$

where $L = r_2 - r_1$, and

$$I = \frac{L}{T_2 - T_1} \ln \frac{T}{T_1}. \tag{84}$$

In Eq. (83), Ei is the exponential integral function of the real argument. The function I_t in Eqs. (16) equals zero in the current thermally stationary case. This solution is inconvenient for practical calculations because it contains nonelementary functions. The UIT approximation gives zero gas velocity. The first-order approximation is defined by the first two terms in Eq. (28). I_J and I are then integrated in elementary functions:

$$I_J^1 = \frac{J_0 R \overline{T}^2}{E} \frac{L}{T_2 - T_1} \left[\exp\left(-\frac{E}{R} \frac{2\overline{T} - T}{\overline{T}^2} \right) - \exp\left(-\frac{E}{R} \frac{2\overline{T} - T_1}{\overline{T}^2} \right) \right] \tag{85}$$

and

$$I^1 = \frac{T_2 - T_1}{2\overline{T}^2} \frac{r^2 - r_1^2}{L} + 2\frac{r - r_1}{\overline{T}} - 2\frac{Tr - T_1 r_1}{\overline{T}^2}. \tag{86}$$

Figure 7(a) presents the gas velocity profiles for numerical simulation in the full Navier-Stokes equation system, for the exact analytical solution and for the first approximation. The numerical simulation is conducted for high Fourier number. The velocity is normalized by a reference value $u_{ref} = L J_0 R T_1 \exp(-E/RT_1)/p_0$. Dimension analysis showed that the system-defining parameters can be reduced to two dimensionless complexes: $\alpha = T_2/T_1$ and $\Theta = E/RT_1$. The numerical solution coincides with the exact analytical solution. The relative error of the first-order approximation is not worse than 15%. The shape of the space profile of the gas velocity is similar to that in the case of heated walls: zero velocity on both boundaries and one extremum in-between. The sign of the velocity is opposite to the sign of the temperature gradient. The maximal velocity decreases in time from the very beginning. In the limit of $\Theta \to 0$, the dimensionless velocity can be approximated by

$$\tilde{u}(\Theta \to 0) = \frac{[1 + (\alpha - 1)x]\{x \ln \alpha - \ln[1 + (\alpha - 1)x]\}}{(\alpha - 1)\tau + \ln \alpha}, \tag{87}$$

where $\tau = J_0 R T_1 t / p_0$.

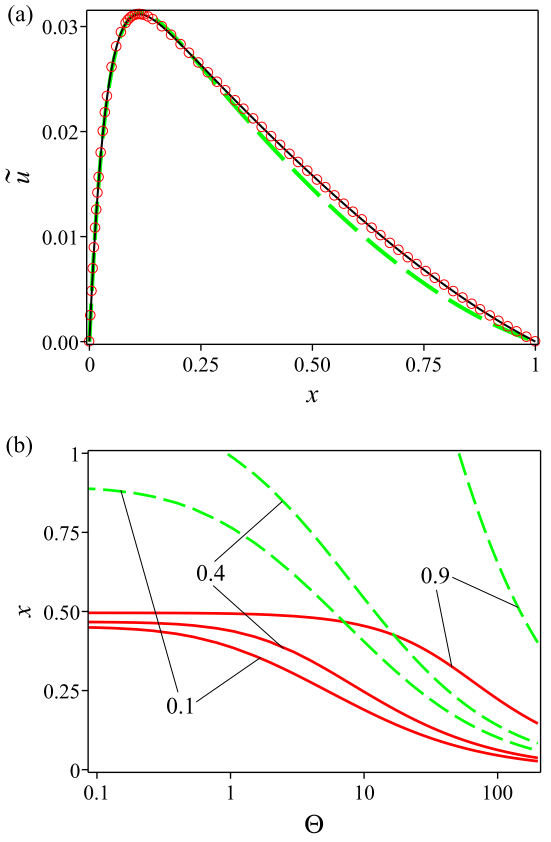

FIG. 7. Distributed mass sources with Arrhenius-type kinetics: (a) Gas velocity profiles obtained from the exact solution (solid black curve), first approximation (dashed green curve), and numerical simulation in ANSYS FLUENT (red circles) at $\alpha = 0.3$, $\Theta = 34$ versus dimensionless coordinate x (42). (b) Velocity extremum location (solid lines) and inflection point location (dashed lines) as functions of Θ at three values of α denoted next to the curves.

The results of the parametric analysis of the velocity profile are shown in Fig. 7(b). At fixed α, the increase of Θ shifts the velocity extremum toward the hot wall, arbitrarily close to it, and decreases the value of the extreme velocity itself. At almost equal boundary temperatures ($\alpha \to 1$) and moderate activation energy ($\Theta < 1$), the extremum point tends to the middle of the gap $X \to \frac{1}{2}$. Unlike the velocity profiles in the case of heating walls, the velocity profiles due to a distributed source get an inflection point in a certain range of parameters. The inflection point is always between the velocity extremum and the cold wall. The larger the α, the narrower the Θ range where the inflection point exists. The latter is illustrated in Fig. 7(b) by the dashed curve for $\alpha = 0.9$. The velocity profiles in the planar geometry ($n = 0$) are qualitatively similar to those in two other geometries ($n = 1,2$).

2. *Heterogeneous mass source (aerosol cloud)*

A nonuniform distributed mass source simulates, particularly, gas absorption or condensation on microparticles. The results are valid for any dimensionality n and may be related to the transition periods in astrophysical [33,36] and complex plasma [34,35] research in microgravity. We suppose that a cloud of size r_c is in the center of a chamber with the size r_2. The cloud particles and the gas are in the state of mass exchange with intensity $J(r,t)$ at uniform temperature $T(t)$. The pressure is defined by expression (81), and the gas velocity follows from Eq. (23) and geometrical factor from Eq. (25) as

$$u = \frac{RT}{p}\left[\frac{I_J}{r^{n+1}} - \frac{I_J(r_2,t)}{r_2^{n+1}}\right]r. \tag{88}$$

Expanding the intensity function in Taylor series near the center, and retaining the zero-order term $J(0,t) \equiv J_0$ in the first integral in the brackets, the gas velocity is

$$u \approx \frac{RTJ_0}{(n+1)p}\left[1 - \frac{n+1}{J_0 r_2^{n+1}} I_J(r_2,t)\right]r. \tag{89}$$

The latter expression has a typical structure for such processes: the gas velocity is directly proportional to the distance from the center and to the volumetric gas production intensity in the central part of the cloud. The velocity is partly compensated by the pressure growth defined by the constant second term in the brackets of Eq. (89).

Peculiarities of the gas velocity profiles clearly follow from the steplike intensity function taken as J_0 for $0 \leqslant r \leqslant r_c$ and as zero for $r_c \leqslant r \leqslant r_2$, giving

$$u = \frac{RTJ_0}{(n+1)p}\begin{cases}\left[1 - \left(\frac{r_c}{r_2}\right)^{n+1}\right]r, & 0 \leqslant r \leqslant r_c \\ \left(\frac{r_c}{r_2}\right)^{n+1}\frac{r_2^{n+1} - r^{n+1}}{r^n}, & r_c \leqslant r \leqslant r_2.\end{cases} \tag{90}$$

Figure 8(a) presents gas velocity profiles in plane geometry ($n = 0$) for clouds of different sizes r_c as compared to the cavity dimension r_2, being used as a filling factor parameter $0 < r_c/r_2 < 1$. An example of such a situation is a dust cloud illuminated by the light sheet resulting in variation of the mass production intensity in the illuminated as compared to nonilluminated region. The coordinate r, in this case, is the distance from the mid-plane of the beam in either directions, and it should always be much smaller than the beam height. Figure 8(b) highlights peculiarities of the profiles with respect to the geometry factor n in a wide cavity ($r_c/r_2 = 0.01$).

Inside the cloud, all the profiles grow linearly. The slope is the highest for all dimensionalities n in an open cavity, $r_c/r_2 \to 1$. In a closed cavity, the slope decreases, while the cloud fills a bigger part of the cavity, and the gas does not move at all when the cloud fills the cavity completely, $r_c = r_2$ [curve 1 in Fig. 8(a)]. The coordinate of the highest gas velocity always coincides with the moving cloud boundary. The velocity attains its maximal value

$$u_{\max} = r_2 \frac{RTJ_0}{p}(n+2)^{-\frac{n+2}{n+1}} \tag{91}$$

when the boundary is located at $r_c/r_2 = (n+2)^{-\frac{1}{n+1}}$, being equal to 0.5 for $n = 0$, to $3^{-1/2}$ for $n = 1$, and to $2^{-2/3}$ for $n = 2$.

In a spherical cavity ($n = 2$), the correction due to the limited dimensions of the cavity is relatively small. Inside the cloud, the correction is defined by the second term in the

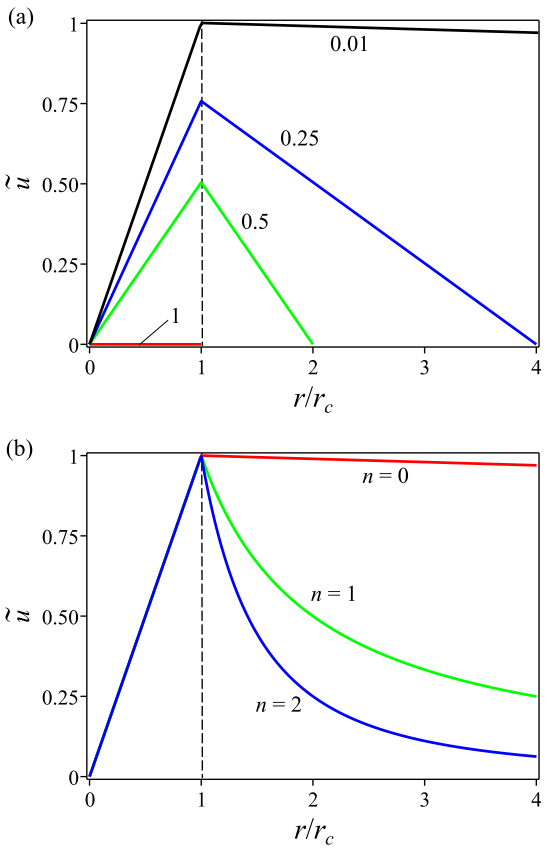

FIG. 8. Gas velocity profiles from Eq. (90) for a steplike function of distributed mass source: (a) parametric dependence on the filling factor r_c/r_2, the values are next to the curves, plane geometry ($n = 0$); (b) parametric dependence on the dimensionality for fixed $r_c/r_2 = 0.01$. All the velocities are normalized by $\frac{r_c R T J_0}{(n+1)p}[1 - (\frac{r_c}{r_2})^{n+1}]$.

brackets of Eq. (90). Already for $r_c/r_2 = \frac{1}{3}$, the correction to the profile in the open cavity is less than 0.04, thus justifying the use of the open cavity approximation ($r_c/r_2 \to 1$) inside and outside the cloud. Realistic profiles of the intensity J are smoother in the region of the cloud boundary. All previous conclusions on the gas velocity profile properties are still valid, keeping in mind that the velocity profiles around the cloud boundary r_c will also be smoother.

From Taylor's decomposition (32), the motion law near the center of symmetry is

$$u \approx \frac{1}{n+1}\left[\frac{\dot{T}_0}{T_0} - \frac{\dot{p}}{p} + \frac{RTJ_0}{p}\right]r. \tag{92}$$

The term $\dot{p}/p$ is negligible for the approximation of an open cavity. The law of motion is simple and universal: the gas velocity is directly proportional to the distance from the element of symmetry. Being periodically modulated, such velocity field creates a central pseudopotential for the particles moving in the gas. It allows to trap them in the same way as realized in the widely used dynamic balancing method [39]. The gas velocity field defined by Eq. (92) is unidirectional in a three-dimensional space, contrary to the particle motion field in the electrodynamic balance characterized by simultaneous contraction-expansion displacement. The latter promises interesting applications of these trapping techniques in aerosol physics.

D. Void cavity with active boundary

In the absence of an internal boundary, the reference boundary becomes a plane of symmetry for $n = 0$, an axis of symmetry for $n = 1$, and a center of symmetry for $n = 2$. The expression for the gas velocity follows straightforwardly from Eq. (17), equating to zero all other functions at $r_1 = 0$:

$$u = \frac{T}{r^n}\left[I_t - \frac{\dot{p}}{p}\int_0^r \frac{\xi^n \mathrm{d}\xi}{T}\right] + \frac{RT}{p}\frac{I_J}{r^n}, \tag{93}$$

where the pressure is defined by Eq. (12) at $r_1 = 0$. The latter expression is useful when the ratio $\dot{p}/p$ may be defined independently in some manner, as was mentioned earlier. Otherwise, relating $\dot{p}/p$ to the parameters of the gas motion sources, the velocity from Eq. (22) and the factor A are

$$u = u_B + u_T + u_J = \frac{T}{T_2}\left(\frac{r_2}{r}\right)^n A\left(\dot{r}_2 - \frac{RT_2}{p}j_2\right) + \frac{T}{r^n}[I_t - AI_t(r_2,t)] + \frac{RT}{pr^n}[I_J - AI_J(r_2,t)], \tag{94}$$

$$A = \left(\int_0^{r_2} \frac{\xi^n d\xi}{T}\right)^{-1} \int_0^r \frac{\xi^n d\xi}{T}. \tag{95}$$

Models without a physical internal boundary simulate different important experimental systems and natural processes, particularly related to the microgravity environment. One example was described in Sec. III C 2. Below, we present some other realizations.

The simplest example is a gas volume inside a cavity. It may be a gas inside a bubble floating in gas or immersed in liquid, a gas inside an elastic balloon, etc. Here, we assume that there are no dispersed second phase or external heat sources modulating temperature and volumetric mass production profiles in the cavity. In this case, all the profiles are uniform in space and may only vary in time, i.e., $T = T(t)$ and $J = J(t)$. The geometrical factor A as defined by Eq. (25) transforms into $A = (r/r_2)^{n+1}$. The second and the third terms in Eq. (94) disappear, and the velocity in the internal region $0 < r < r_2$ reduces to

$$u = u_B = \frac{r}{r_2}\left(\dot{r}_2 - \frac{RT}{p}j_2\right). \tag{96}$$

The gas velocity grows linearly from zero on the element of symmetry to the boundary gas velocity, irrespective of the dimensionality parameter n. It is interesting to note that the velocity in Eq. (66) does depend on the dimensionality parameter n in the presence of the internal boundary (see Fig. 6). From Eq. (96), we receive an obvious but important observation for verification purposes: no gas motion occurs in a cavity with uniform variation of temperature $T = T(t)$, mass production intensity $J = J(t)$, and with boundary conditions $\dot{r}_2 = 0$, $j_2 = 0$.

A syringe-type geometry gives an example of the realization of a flat slot cavity $n = 0$, when the distance between the moving piston and the opposite wall is much smaller than the

diameter. The gas far from the side walls moves according to Eq. (96). It is important to note that the plane of symmetry here is the virtual plane at equal distance from the piston and the opposite wall. The plane of symmetry, therefore, moves with a velocity twice as low as that of the piston in the frame of the syringe. It is the distance from the moving symmetry plane that denotes r.

Axisymmetric geometry $n = 1$ may be illustrated by the radial gas motion inside a tube with the gas passing through permeable walls. The velocity is defined by Eq. (96) for $\dot{r}_2 = 0$.

In a spherical geometry $n = 2$, it may be a balloon or a bubble with inside gas motion defined by Eqs. (93), (94), or (96), in the simplest case. Abrupt evaporation from the walls inside a spherical cavity was used in one of the methods to measure evaporation and condensation coefficients [30]. According to the experimental procedure, the chamber radius was less than 100 mm and total pressure was lower than 1 Pa. The chamber was thermally stabilized, and then the temperature rapidly rose or fell to different values, resulting in evaporation or condensation of the investigated substance deposited on the internal chamber surface. The conditions corresponded to high Fourier number. Expression Eq. (96) with $\dot{r}_2 = 0$ describes gas motion velocity in the cavity. The pressure dependence on temperature is an independent experimental function in such experiments and, therefore, the gas velocity may be calculated alternatively using Eq. (93) for $J = 0$.

IV. DISCUSSIONS

In view of the wide diversity of the phenomena and of the particular realizations of one-dimensional homobaric flows treated in the paper, it seems reasonable to highlight the main features of the system, the model, and the solutions as well as commenting on the model limitations.

A. Peculiarities of the system

1. Task geometry

We studied one-dimensional cases in which the gas flow may only be normal to the boundaries. This condition imposes the following topological limitations on the possible arrangement of the gas volume. Generally, there should be two nonintersecting surfaces: parallel for $n = 0$, coaxial for $n = 1$, and concentric for $n = 2$. For coaxial and concentric geometry, we may distinguish internal boundaries r_1 and external boundaries $r_2 > r_1$. One of the boundaries for $n = 0$ as well as the external boundary for $n = 1$ and 2 may be treated formally as being at infinity. However, in this approximation, the zone of the model validity only will be near the internal boundary, giving an outside nonphysical solution. The internal boundaries for $n = 1$ or 2 will "disappear" for $r_1 = 0$, being transformed into an axis or a center of symmetry, respectively. For $n = 0$, it will be an infinite slot with a plane of symmetry at the origin $r_1 = 0$ and the external boundary at r_2. This case is similar to the usual plane task with identical boundary conditions at r_2 and $-r_2$.

2. Model assumptions

The basic assumption of the current model is the uniformity of the gas pressure, applicable when the reference times of all the processes in the system are much longer than the acoustic time. Mathematically, it is valid at small Mach numbers $\mathrm{Ma} \ll 1$. In one-dimensional geometry, it allows the gas velocity to be obtained using the mass conservation condition and the equation of state without solving the momentum equation.

If the gas flow has a component due to temperature variation, the energy equation must be solved. In the current model, it is reduced to the heat equation, which does not contain gas velocity. After the analytical expressions for the velocity are obtained as in Sec. III A, the validity of this assumption can be proved directly as follows. For the flat geometry, the maximal possible velocity is estimated from Eq. (45) as $u_{\max} < \dot{T}_{\max} L/4\overline{T}$ for $\dot{T}_1 = -\dot{T}_2 = \dot{T}_{\max}$. Considering that $\dot{T}_{\max} \approx \Delta T_{\max}/\Delta t_{\min} = \chi \Delta T_{\max}/\mathrm{Fo}\, L^2$, the estimate of the maximal Peclet number in quasistationary regime gives $\mathrm{Pe}_{\max} = u_{\max} L/\chi \leqslant \Delta T_{\max}/4\mathrm{Fo}\, T \ll 1$. Hence, the influence of advection defined by the second term on the left-hand side of the energy equation (6) is negligible. In axisymmetric and centrosymmetric geometries, the maximal velocities are even lower, as shown in Fig. 4(b). The inequality is more pronounced in the nonstationary regime, as illustrated in Figs. 2(b) and 3(b).

At high Fourier number, the pressure variation term can be neglected in the energy equation. The influence of the pressure variation may be very low in the following practical cases: in flat geometry when the temperature variation on the two boundaries is equal but of opposite sign; in axisymmetric and centrosymmetric geometry when the active zone is concentrated near the internal boundary; and near the element of symmetry when the extension of the zone is sufficiently smaller than the dimension of the whole region.

In certain cases, especially in practical applications, the model still may be valid in the region of interest in spite of the outer region properties not obeying the limitations of the current model. Particularly, the gas flow outside the reference volume may not be one dimensional. The current model still will be valid as far as it is possible to define the gas pressure p and its time derivative $\dot{p}$ in the reference $[r_1, r]$ region. Experimentally, it may be realized, for example, by pressure measurements.

3. Solution method

To find the gas velocity u, we introduce a virtual surface at a distance r from the reference boundary to define the volume, to which the mass conservation law is applied. The local gas velocity u thus coincides with the velocity of the virtual surface $\dot{r}$. The pressure is defined from the mass conservation law for the whole domain; being uniform, it does not require spatial integration. After these transformations, the velocity and the pressure are expressed through the integrals with respect to r of the functions of temperature profiles and eventual distributed mass sources. The solution procedure is completed by finding temperature profiles from the heat equation and substituting them into the integrals.

It is a matter of convenience to choose one or another boundary as a reference in addition to the virtual surface. Typically, we choose the internal boundary. It is noteworthy that the expressions for the gas velocity, as for example Eq. (17), contain only characteristics defined in the reference

region, here in $[r_1, r]$. Whatever happens outside the reference region is taken into account by the uniform gas pressure p and its time derivative $\dot{p}$. They may be explicitly expressed through the characteristics of the whole $[r_1, r_2]$ region from Eq. (12).

4. Velocity profile shapes

The variety of velocity profiles for $\mathrm{Fo} \gg 1$ are illustrated in Fig. 1. When boundary temperature variation in time is the only source of gas motion, the velocity profiles are always as in Figs. 2 and 4 having zero on the boundaries and one extremum in-between. One of the most illustrative and useful results is the expression for the gas velocity in the flat gap of width L between two walls with varying temperatures T_1 and T_2 expressed in UIT approximation from Eq. (45) as

$$u_{\mathrm{UIT}} = \frac{\dot{T}_2 - \dot{T}_1}{T_1 + T_2}(x-1)xL, \quad x = \frac{r - r_1}{L}, \tag{97}$$

where r_1 is the coordinate of the left wall. The velocity profile is parabolic, with the maximum $u_{\max} = (\dot{T}_2 - \dot{T}_1)L/8\bar{T}$. The solution is applicable to the thin layer in axisymmetric and centrosymmetric geometries as well. We refer to the Supplemental Material presenting the animated solution for the velocity.

In the presence of distributed sources, there may appear a flex point shifted toward the internal boundary for cylindrical and centrosymmetric geometries, as in Figs. 1(d) and 8.

5. Significance and maximal effects

Significance of the flows under consideration depends upon objectives of the task. Even gas velocity as low as one micrometer per second may be of crucial importance in the investigation of transport phenomena, particularly studying the negative thermophoresis of aerosol particles [27,28]. It is of interest, however, to identify the systems and parameters that result in the highest possible velocities and gas displacement. Generally, this will be accomplished on the way to maximizing the spatial nonuniformity, increasing the rate of its variation and the extension of the "active" zone. For the order-of-magnitude analysis, we rewrite Eq. (92) as

$$u \approx \frac{1}{n+1}\frac{l_{\max}}{\Delta t}\left[\frac{\Delta T}{T} + \frac{\Delta m_g}{m_g} - \frac{\Delta p}{p}\right], \tag{98}$$

where $l_{\max}$ is the extension of the zone of most intensive gas density variation during Δt, as a result of deviation of temperature ΔT and mass Δm_g in the reference volume, and of the overall pressure Δp in the system.

Although Eq. (92) is obtained for the systems with the element of symmetry as the internal boundary, it is also relevant when the internal boundary exists but does not move and there is no mass sources on it. If the internal boundary does move, the origin of the coordinates should be placed on the moving boundary. Expression (98), being transformed in the form $u\Delta t/l_{\max}$, defines the estimate of the total maximal relative expansion and contraction of the zone of most active gas density variation.

Moving boundaries vary pressure and result in gas displacement according to Eqs. (66)–(69), with velocities that may attain subsonic values. Gaining high velocities due to temperature variation is also possible in a homogeneous fixed-volume system as well as in the systems with distributed sources of gas motion. Here is an example of maximal velocity estimation in a homogeneous fixed-volume system for a flat slot, $n = 0$, with two walls at a fixed distance L. One wall is heated so that its initial temperature T increases by ΔT during Δt. Variation of temperature profile results in gas motion with the velocity in the maximum that we express through the Mach number as $c\mathrm{Ma}$. Supposing that the temperature profile variation is the only reason for the gas motion, the order-of-magnitude estimate from Eq. (98) gives the relation between the temperature growth rate and other system parameters as $\Delta T/\Delta t \approx c\mathrm{Ma}T/l_{\max}$. For a slot dimension $l_{\max} = 0.1$ m, ambient temperature $T = 300$ K, and $\alpha_c = 0.003$ corresponding to the maximal gas velocity 1 m s^{-1}, the order of magnitude estimate gives $\Delta T/\Delta t \approx 3000$ K s^{-1}, which is a quite realistic value for millisecond heating processes. The exact solution (44) and very accurate UIT approximations from Eq. (45) require about an eight times higher temperature growth rate. This discrepancy is because the pressure variation in Eq. (98) in the above estimate was neglected.

B. Beyond the model limitations

1. Local one dimensionality

Only rare real-life systems are strictly one dimensional. The model, however, may be used to estimate the maximal effects or to obtain accurate local approximations. Some examples are presented in Sec. I B. In Ref. [9] it is noted that the homobaric approximation may be applied to the two-dimensional boundary layer problem to find components perpendicular to the layer.

The break of symmetry due to gravity may be neglected for sufficiently small system dimensions, low pressure, and/or rapid processes, such as droplet ignition. We expect that the current model may be applied for local estimates of rather complicated phenomena, such as vertical motion in heated or cooled atmosphere [40], replacing molecular kinetic coefficients by the effective parameters by considering turbulence, altitude dependencies, etc.

2. Superposition of flows

To a certain extent, the current model may be applied to essentially asymmetric systems. Suppose that we have a set of gas motion sources inside a spherical cavity with neutral outer boundary. This paper provides analytical solutions only for a single source with central symmetry. To obtain a quantitative outlook, we compared results of the full-scale numerical simulation with the estimates based on the analytical solutions for the following system. Two small spheres with radii r_S and temperatures $T_1(t)$ and $T_2(t)$ are placed in a spherical cavity with outer radius R and temperature T_0. The small spheres are located equidistantly with respect to the cavity center at $2l$ between their centers.

Numerical simulation was conducted using ANSYS FLUENT for $R = 50r_S$, $l = 5r_S$, $T_1(t) = T_2(t) = T_0 + kt$. The gas pressure value was chosen sufficiently low to meet the requirement $\mathrm{Fo} \gg 1$ for a quasistationary temperature distribution.

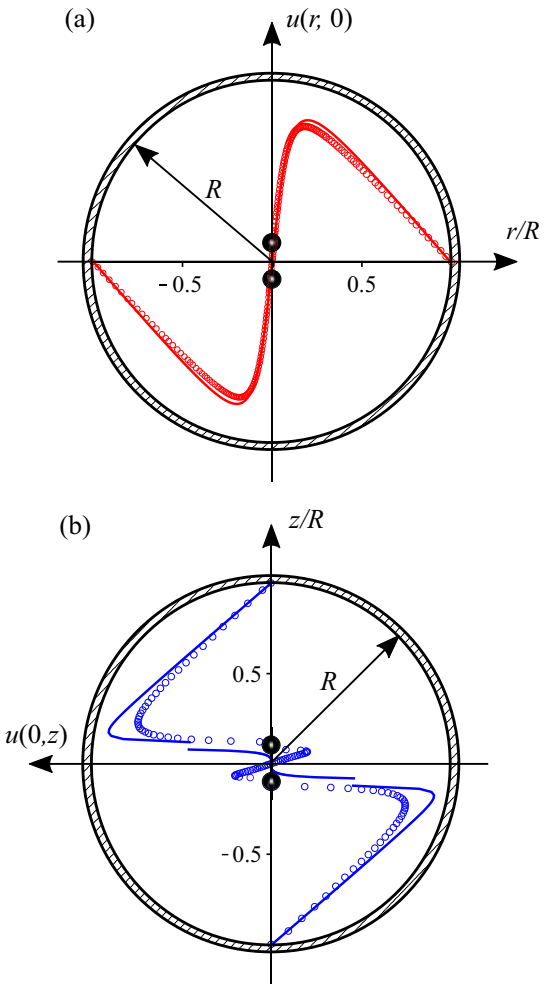

FIG. 9. Gas flow generated by two small heating spheres inside a spherical cavity at $t = 0.05T_0/k$. Hollow circles for numerical velocity profiles and solid lines for superposition of two analytical solutions: (a) radial components $u(r,0)$ along the axis in the equatorial plane and (b) axial components $u(0,z)$ along the axis through the sphere centers.

The analytical estimate is based on the solution for a small sphere with the previously mentioned characteristics placed exactly in the cavity center (see Sec. III A). Gas velocity for a combination of two spheres is calculated as a vector sum of the two solutions. The comparison of the analytical and numerical profiles are in Fig. 9, where the dimensions of the cavity, the small spheres, and the distance between them are in the same scale.

In the equatorial plane, the $u(r,0)$ numerical and analytical solutions are in very good agreement, as shown in Fig. 9(a). The maximum discrepancy is 5% near the extremum of the velocity profiles, which is at a distance of about $2l = 10r_S$. It is not a surprise that the $u(0,z)$ velocity components of analytical and numerical solutions between the spheres $(-l + 0.5r_S) \leqslant z \leqslant (l - 0.5r_S)$ have nothing to do with each other, as shown in Fig. 9(b). However, in the outside region for $|z| \geqslant (l + 0.5r_S)$, the solutions are comparable with a maximum discrepancy of 18% on the extremum of the velocity profile, again at approximately the distance between the spheres.

The example shows that the superposition principle gives quite an accurate estimate of the resultant gas velocity in the region outside the sources, in the cases when the sources are sufficiently small, far from each other as well as from the outer boundary, and quite close to the element of symmetry.

3. *One-dimensional shear flows*

Here, the flow is unidirectional, but the flow rate is not uniform laterally. Suppose two infinite plates are parallel to z, with varying-in-time, antiparallel temperature gradients along the plates: $T_1(z) = T_0 + C(t)z$ and $T_2(z) = T_0 - C(t)z$. The position and the value of the maximal flow velocity are defined by Eqs. (46) and (47). The maximal flow velocity is approximately in the middle between the planes, and from Eq. (45) it is estimated as $u(x_{\max},z) \approx -zC(t)(r_2 - r_1)/4\bar{T}_0$, giving uniform shear flow $\partial u/\partial z$.

V. CONCLUSIONS

In this paper, we presented a class of analytical solutions of gas velocity profiles for one-dimensional creeping flow in the approximation of uniform pressure. The general solution was obtained for the flows between two boundaries in planar, axial, and central symmetries for different types of motion sources. The latter comprised the boundary time-dependent temperatures $T_i(t)$ and heat fluxes $q_i(t)$, boundary motion $\dot{r}_i(t)$ and mass sources $j_i(t)$, distributed mass $J(r,t)$, and heat sources $Q(r,t)$.

We demonstrated that within the limitations of the model, the exact analytical solutions were identical to the numerical results obtained on the basis of the full system of the Navier-Stokes equations in the computational fluid dynamics software ANSYS FLUENT.

In view of the immense variety of particular cases, we restricted ourselves to finding analytical solutions and analyzing them for a set of representative tasks limited by quasistationary heat transfer (Fo $\gg$ 1), with Poisson equation for temperature. Particular solutions are presented in three categorizing tables for planar, axial, and central symmetries. The elements of Table I give references for the sections with appropriate solutions. Gas motion sources were combined in three groups per expression (23) (i.e., boundary, thermal, and distributed mass sources). References on the cases with single active sources are in the diagonal table elements. Solutions describing combined action of two sources occupy nondiagonal elements. A table with all combinations of task characteristics, is not appropriate for the current publication because it would be multidimensional and would contain hundreds of elements.

Most studied in this paper are the particular cases with single motion source: temperature profile variation. The problems are solved for all three types of symmetry and two types of boundary conditions: periodic and linear temperature variation. The variety of velocity profiles may be reduced to a simple hump-shaped curve, always having zero velocity on the boundaries, with one extremum in-between as it is illustrated by the animation in the Supplemental Material. The extremum location depends on the boundary temperature ratio and on the wall radius ratio (in nonplanar geometries). In planar geometry, at moderate difference between the boundary temperatures, velocity profiles are close to parabola, with the extremum

TABLE I. Categorizing table of solutions, including types of symmetry and motion sources. Table elements provide references to the corresponding formulas in the paper.

$n=0$				$n=1$				$n=2$			
	u_T	u_B	u_J		u_T	u_B	u_J		u_T	u_B	u_J
u_T	(44)	(44), (72)		u_T	(57)			u_T	(62), (37)		
u_B		(66)		u_B		(66), (97)		u_B		(66), (96)	
u_J			(80), (83), (84); (90)	u_J			(90)	u_J			(90)

around the mid-plane. It is shown that the gas flows in one direction in the whole domain at any moment for all three types of symmetries.

The general solution for both boundary displacement and boundary mass sources is obtained for arbitrary geometry under the assumption of temperature uniformity. The two effects are combined in one solution because they produce similar velocity profiles. Instantaneous velocity profile has a nonzero value, at least on one of the boundaries, and approaches the opposite boundary value by law $\varphi(G)r + \psi(G)/r^n$, where a linear component prevails at extreme values of the wall radius ratio G. A single stagnant point (velocity equal to zero) can appear in the domain, for example, in the case of gas inflows on both boundaries.

As an example of combined action of two motion source, a flow induced by simultaneous motion and heating of one of the boundaries is considered in a planar gap. The contributions of both motion sources in this particular case are additive: velocity is a sum of one term due to gas heating and another term due to the wall displacement. A stagnant point can appear when the wall moves out of the domain and its temperature grows at the same time (or vice versa).

Distributed mass sources are presented in two particular solutions. In the first solution, in a planar geometry, the source intensity depends on temperature according to Arrhenius law, while the temperature profile remains stationary. The velocity profile is similar to that in the task with heating walls, but it can have an inflection point depending on the temperature difference and the activation energy. In the general case, the profiles may acquire multiple flex points as well as additional local extrema and/or zeros. The second solution describes isothermal mass production in the central part of a domain without an inner boundary. It is shown that the velocity grows linearly in the mass-producing region, while outside it decreases as $1/r^n$.

We proposed a simple estimation of the maximal gas velocity (98), which may attain high values. The boundaries of the stability for the flow patterns should still be evaluated. Upon taking adequate precautions, the results may be used beyond the model limitations. Thus, flow one dimensionality may be sufficient only locally; in certain complex systems, the velocity may be well approximated by the superposition of the velocities from a series of independent sources. This approach may be applied to some uniform shear flows.

We proposed using the uniform inversed temperature (UIT) approximation in denominators of the integrals in general solution. It made analytics much easier, while the solutions were still accurate and their interpretation was much clearer. Exact solutions for boundary time-dependent temperatures $T_i(t)$ in the quasistationary regime of heat transfer were compared with the numerical calculations in transition ($\mathrm{Fo} \approx 1$) and essentially nonstationary ($\mathrm{Fo} \ll 1$) regime of heat transfer. The differences between solutions are found to be negligible for $\mathrm{Fo} > 10$. The corrections become noticeable for $\mathrm{Fo} \approx 1$, attaining about 0.03 of the maximal velocity values and quickly growing for lower Fourier number so that the quasistationary approximation gives more than twice higher velocities for $\mathrm{Fo} = 0.1$. Analytical solutions and the analysis of the velocity profiles in the essentially nonstationary regime will be presented in a separate publication. The analytical solutions may be used as reference in validating numerical methods for slow flows in compressible fluid dynamics.

We anticipate the application of the results in planning and processing of the experiments dealing with high accuracy measurements of the kinetic coefficients and transport properties of suspended particles, especially in microgravity conditions. The results may be useful in the evaluation of pertinent gas creep components in single bubble dynamics, condensation and evaporation phenomena, droplet burning, etc.

Periodic processes should be of practical interest in aerosol mechanics and dust cloud manipulation. Close to the boundary (32) or element of symmetry (92), the gas velocity grows linearly with the distance. Being periodically modulated, such flow results in a secular drift of particles suspended in the gas, giving rise to such applications as promoting particle deposition, jet focusing, and growth of cloud particle number concentration in a spherically symmetric confining pseudopotential.

The approach of this paper may be extended to other compressible fluids with different equations of state, allowing study of motion in nonideal gases, liquids, or solid elastic media. The model may be generalized for multicomponent gases, considering gas density variation because of diffusion and chemical reactions.

The authors expect that the simplicity of the model, clear physical meaning, and wide variety of possible particular cases will make it useful in university class works, especially with use of symbolic computation software.

ACKNOWLEDGMENT

Belgian Science Policy Office and European Space Agency PRODEX Programme are kindly acknowledged for their support.

[1] L. Rayleigh, Philos. Mag. **47**, 314 (1899).

[2] B. Larkin, in *2nd Thermophysics Specialist Conference, New Orleans, LA, USA, Fluid Dynamics and Co-located Conferences* (Martin Marietta Corp., Martin Co., Denver, Colo), doi: 10.2514/6.1967-337.

[3] A. M. Radhwan and D. R. Kassoy, J. Eng. Math. **18**, 133 (1983).

[4] D. R. Kassoy, SIAM J. Appl. Math. **36**, 624 (1979).

[5] S. Paolucci, *Filtering of Sound from the Navier-Stokes Equations* (Sandia National Laboratories, Livermore, CA, 1982).

[6] D. A. Nikulin and M. K. Strelets, High Temp. **22**, 707 (1984).

[7] A. E. Kuznetsov, O. A. Nekhamkina, and M. K. Strelets, High Temp. **22**, 862 (1984).

[8] D. V. Agafonov and S. G. Cherkasov, High Temp. **40**, 571 (2002).

[9] S. G. Cherkasov, High Temp. **48**, 422 (2010).

[10] S. G. Cherkasov and V. V. Mironov, Bull. Russ. Acad. Sci. Energetics **61**, 134 (2012).

[11] Y. V. Lapin and M. K. Strelets, *Internal Gas Mixtures Flows* (Nauka, Moscow, 1989), p. 368.

[12] See Supplemental Material at http://link.aps.org/supplemental/10.1103/PhysRevE.94.053121 for an animated solution of the gas flow in a planar gap.

[13] S. Ostrach, Bull. Mater. Sci. **4**, 109 (1982).

[14] P. G. Grodzka and T. C. Bannister, Science **176**, 506 (1972).

[15] P. G. Grodzka and T. C. Bannister, Science **187**, 165 (1975).

[16] P. Guenoun, B. Khalil, D. Beysens, Y. Garrabos, F. Kammoun, B. Le Neindre, and B. Zappoli, Phys. Rev. E **47**, 1531 (1993).

[17] B. Zappoli, D. Bailly, Y. Garrabos, B. Le Neindre, P. Guenoun, and D. Beysens, Phys. Rev. A **41**, 2264 (1990).

[18] A. Toda, Y. Ohi, R. Dobashi, T. Hirano, and T. Sakuraya, J. Chem. Phys. **105**, 7083 (1996).

[19] A. Toda, H. Ohnishi, R. Dobashi, T. Hirano, and T. Sakuraya, Int. J. Heat Mass Transfer **41**, 2710 (1998).

[20] W. Oostra, An experimental approach into the phenomenon of thermophoresis, Ph.D. thesis, Delft University of Technology, 1998.

[21] W. Oostra, J. C. M. Marijnissen, and B. Scarlett, Space Forum **3**, 251 (1998).

[22] H. Ono, R. Dobashi, and T. Sakuraya, Proc. Combust. Inst. **29**, 2375 (2002).

[23] A. A. Vedernikov, F. Prodi, G. Santachiara, S. Travaini, F. Dubois, and J. C. Legros, Microgravity Sci. Technol. **17**, 102 (2005).

[24] F. Prodi, G. Santachiara, L. Di Matteo, A. Vedernikov, S. A. Beresnev, and V. G. Chernyak, J. Aerosol Sci. **38**, 645 (2007).

[25] F. Prodi, G. Santachiara, S. Travaini, A. Vedernikov, F. Dubois, C. Minetti, and J. C. Legros, Atmos. Res. **82**, 183 (2006).

[26] B. R. Mohd Azahari, M. Mori, M. Suzuki, and W. Masuda, J. Aerosol Sci. **54**, 77 (2012).

[27] S. A. Beresnev, A. Vedernikov, and A. Markovich, Atmos. Oceanic Opt. **21**, 508 (2008).

[28] A. Vedernikov, S. A. Beresnev, and A. Markovich, J. Jpn. Soc. Microgravity Applicat. **23**, 267 (2008).

[29] D. L. Dietrich, V. Nayagam, M. C. Hicks, P. V. Ferkul, F. L. Dryer, T. Farouk, B. D. Shaw, H. K. Suh, M. Y. Choi, Y. C. Liu, C. T. Avedisian, and F. A. Williams, Microgravity Sci. Technol. **26**, 65 (2014).

[30] S. A. Kitchener and R. F. Strickland-Constable, Proc. R. Soc. A: Math. Phys. **245**, 93 (1958).

[31] A. A. Aganin, Int. J. Numer. Methods Fluids **33**, 157 (2000).

[32] I. Akhatov, O. Lindau, A. Topolnikov, R. Mettin, N. Vakhitova, and W. Lauterborn, Phys. Fluids **13**, 2805 (2001).

[33] J. Blum and G. Wurm, The growth mechanisms of macroscopic bodies in protoplanetary disks, in *Annual Review of Astronomy and Astrophysics*, Vol. 46 (Annual Reviews, Palo Alto, CA, 2008), pp. 21–56.

[34] V. E. Fortov, A. V. Ivlev, S. A. Khrapak, A. G. Khrapak, and G. E. Morfill, Phys. Rep. **421**, 1 (2005).

[35] G. E. Morfill and A. V. Ivlev, Rev. Mod. Phys. **81**, 1353 (2009).

[36] J. Blum, A. C. Levasseur-Regourd, O. Muñoz, R. J. Slobodrian, and A. Vedernikov, Europhys. News **39**, 27 (2008).

[37] A. Vedernikov, N. Freuville, D. Balapanov, and A. Cecere, in *Proceedings of 63rd International Astronautical Congress, IAC, Vol. 2, Naples, Italy, 2012* (International Astronautical Federation, Paris, 2012), pp. 777–787.

[38] C. Geuzaine and J.-F. Remacle, Int. J. Numer. Methods Eng. **79**, 1309 (2009).

[39] W. Paul, Rev. Mod. Phys. **62**, 531 (1990).

[40] J. M. Wallace and P. V. Hobbs, in *Atmospheric Science*, 2nd ed. edited by J. M. Wallace and P. V. Hobbs (Academic, San Diego, 2006), pp. 271–311.